

RESEARCH ARTICLE

10.1002/2017TC004562

Key Points:

- A newly recognized ~2730 Ma regional unconformity in the Yilgarn Craton developed during syntectonic emplacement of the Yarraquin pluton
- These two events reflect an ~2730 Ma regional deformation event marking the onset of the Neoarchean Yilgarn Orogeny
- This orogeny ended a 200 Myr phase of prevailing extension marked by the deposition of a deep marine greenstone sequence

Supporting Information:

- Supporting Information S1
- Table S1
- Table S2
- Table S3

Correspondence to:

I. Zibra,
ivan.zibra@dmp.wa.gov.au

Citation:

Zibra, I., F. Clos, R. F. Weinberg, and M. Peternell (2017), The ~2730 Ma onset of the Neoarchean Yilgarn Orogeny, *Tectonics*, 36, 1787–1813, doi:10.1002/2017TC004562.

Received 10 MAR 2017

Accepted 27 JUL 2017

Accepted article online 10 AUG 2017

Published online 18 SEP 2017

The ~2730 Ma onset of the Neoarchean Yilgarn Orogeny

I. Zibra^{1,2} , F. Clos², R. F. Weinberg² , and M. Peternell³ 
¹Geological Survey of Western Australia, East Perth, Western Australia, Australia, ²School of Earth, Atmosphere and Environment, Monash University, Clayton, Victoria, Australia, ³Institute of Geosciences, University of Mainz, Mainz, Germany

Abstract The timing of the onset of an orogeny is commonly constrained indirectly, because early orogenic structures are rarely exposed or are overprinted. Establishing the onset of an Archean orogeny is considerably more challenging, because of the more fragmented geological record and the general lack of consensus about Archean geodynamics. We combine existing tectonostratigraphic data with new structural and geophysical data sets to establish the onset of the Neoarchean Yilgarn Orogeny (Yilgarn Craton, Western Australia). We show that the surface of the ~2960–2750 Ma deep-marine Yilgarn greenstone sequence was uplifted, eroded, and unconformably overlain by an ~2730 Ma, syntectonic clastic sequence, deposited in shallow marine to subaerial conditions, and derived from the erosion of the underlying greenstones. This ~2730 Ma regional unconformity predates the oldest known Yilgarn structures; therefore, its tectonic significance is so far unknown. At around the same time, at deeper crustal levels, the ~2728 Ma Yarraquin pluton was being emplaced along an active, large-scale shear zone network. Our mesostructural and microstructural analysis shows that the bulk of the fabric in the granite and its country rocks developed during pluton emplacement and was largely assisted by magma-present shearing. Overall, these structures reflect an important event of synemplacement crustal shortening. The regional unconformity and the syndeformational emplacement of the Yarraquin pluton are both expressions of an ~2730 Ma regional deformation event associated with significant crustal thickening, marking the onset of the Neoarchean Yilgarn Orogeny.

1. Introduction

The term orogeny was first introduced to describe processes related to elevation of the surface of the Earth as a result of crustal deformation [Gilbert, 1890] and has been progressively modified to include additional geological processes, such as rock deformation, sedimentation, metamorphism, and magmatism (see Schellart and Rawlinson [2010] for a review). The early stages of an orogenic cycle are typically characterized by the development of an orogenic wedge, located between the subducting plate and the overriding continental margin [Vanderhaeghe, 2012]. Contractual structures developed at such an early stage (i.e., at the onset of an orogeny) tend to be elusive, because of subsequent tectonic overprinting or simply because not recorded by the younger rocks exposed. Even in the European Alps—possibly the most extensively studied mountain belt—after a century and a half of detailed structural work, the timing of the onset of the orogeny is still a matter of debate [Stampfli et al., 2002; Handy et al., 2010]. The onset of orogeny is often constrained indirectly, for instance, from the synorogenic stratigraphic record [Dieni and Massari, 1982; Garzanti et al., 1987; DeCelles et al., 2004; Hu et al., 2015] or through multidisciplinary studies based on stratigraphic, palaeomagnetic, and geochronological data [Boger and Miller, 2004; Chew et al., 2007; Najman et al., 2010].

Uncertainties about timing of orogeny onset increase dramatically for Archean orogens, owing to the more fragmented geological record and the general lack of consensus about Archean geodynamics [Condie and Benn, 2006; van Hunen et al., 2008; Gerya, 2014]. Moreover, since the association of granites with volcano-sedimentary supracrustal sequences has no Phanerozoic counterparts, the tectonic setting of Archean granite-greenstone terranes is highly debated [Hamilton, 1998; Bédard et al., 2013]. Despite these uncertainties, the geological record preserved in greenstone belts represents a vast source of information for the understanding of Archean tectonics.

Two main end-member types of Archean greenstone sequences are commonly recognized. Laterally extensive mafic-ultramafic volcanic sequences (70–90% of the thickness of greenstone belts [Bédard et al., 2013]), intercalated with chemically precipitated banded iron formations (BIFs), were deposited in deep marine environments (shield volcanoes or “mafic plains” [Condie, 1990; Thurston and Chivers, 1990]), away from any detrital input from emerged continents [Klein, 2005; Thurston et al., 2012]. They represent tectonically

or subsidence-controlled basins that developed over long periods of lithospheric thinning [Flament *et al.*, 2011]. In tectonically active regions, clastic sequences were deposited in narrow basins, rapidly filled with proximal sediments, in subaerial to shallow marine environments [Lamb, 1987; Mueller and Corcoran, 1998; Krapež and Barley, 2008]. They unconformably overly both older deep-marine greenstone sequences and granitic rocks, from which the clastic material was sourced [Thurston and Chivers, 1990; Morris *et al.*, 2007], reflecting periods of intense surface uplift and erosion [Krapež and Barley, 2008]. Despite Archean unconformities evidently marking a significant change in tectonic regime, their tectonic significance is poorly understood [Corcoran and Mueller, 2007].

Greenstones from the Neoarchean Yilgarn Orogen (Western Australia) contain remnants of an ~2730 Ma unconformity [Morris *et al.*, 2007] predating the oldest-known contractional structures (dated at ~2700 Ma [Zibra *et al.*, 2014b; Cohalan *et al.*, 2015]). Thus, it is not known whether this unconformity reflects a period of extensional or contractional tectonic activity and whether this erosional surface represents local and independent episodes of basement uplift forcing surface uplift, for instance, related to episodic gneiss dome emplacement [Collins, 1989] or a regional feature related to large-scale tectonic events.

The first part of this paper outlines the tectonostratigraphic evolution of greenstones from the western part of the Yilgarn Orogen, with particular reference to the ~2730 Ma time slice. The synthesis of the literature suggests that the sparsely preserved, ~2730 Ma clastic sedimentary rocks are remnants of a regional (≥ 400 km-wide) unconformity. The second part presents a structural study of a newly discovered, large-scale transpressional shear zone network along which the ~2728 Ma synkinematic Yarraquin pluton was emplaced. Importantly, this is the oldest-known shear zone network in the Yilgarn Orogen. We couple these independent sets of data to show that the emplacement of the Yarraquin pluton and the ~2730 Ma regional unconformity are different expressions of the first, large-scale event of horizontal shortening recorded in the Yilgarn crust, marking the onset of the Neoarchean Yilgarn Orogeny.

2. Regional Geological Setting

The Archean Yilgarn Craton of Western Australia is a wide granite-greenstone terrain that formed mainly in the ~3050–2600 Ma time span, with a minor older component up to >3700 Ma, preserved in its north-west part (Figures 1a and 1b) [Wyche, 2007]. Lu-Hf data reveal that the craton experienced several major events of crust generation from at least ~4200 Ma [Wyche *et al.*, 2012]. Geophysical and structural data indicate that the whole craton includes a network of E dipping, crustal-scale shear zones, locally associated with upper crustal, W dipping shear zones (Figure 1c) [Wilde *et al.*, 1996; Drummond *et al.*, 2000; van der Velden *et al.*, 2006; Zibra *et al.*, 2014b]. Based on field data and analysis of geological maps, such shear zone network has been described as a system of conjugate strike-slip shear zones (Figure 1), with NE trending dextral and NW trending sinistral segments, joined by areas dominated by coaxial deformation [Vearncombe, 1998; Chen *et al.*, 2001]. As a whole, this network reflects long-lasting E-W shortening during the ~2700–2630 Ma Neoarchean orogeny [Vearncombe, 1998].

The tectonic evolution of the craton is a matter of long-standing debate, and tectonic models range from arc-accretion [Barley *et al.*, 1989, 2008; Myers, 1995; Qiu and Groves, 1999; Czarnota *et al.*, 2010; Morris and Kirkland, 2014] to autochthonous (i.e., plume-dominated [Wyche *et al.*, 2012; Van Kranendonk *et al.*, 2013]). In analogy to other cratonic blocks assembled during the Neoarchean, the occurrence of gently dipping reflectors throughout the Yilgarn Orogen (Figure 1c) likely reflects deformation processes dominated by horizontal shortening and plate interactions [van der Velden *et al.*, 2006]. This marked, middle to lower crustal seismic reflectivity is likely due to layered migmatitic complexes developed along magma transfer zones, during the assembly of the main syntectonic plutons [Zibra *et al.*, 2014b]. The overall architecture, lithological association, and tectonomagmatic evolution of the Yilgarn Orogen are comparable to that of the Neoarchean Superior Province of Canada [Cruden *et al.*, 2006], which likely formed by progressive Neoarchean accretion of juvenile volcanic arcs and continental crustal fragments onto a Mesoarchean nucleus [Percival *et al.*, 1994].

The Yilgarn Craton is subdivided into Youanmi Terrane and Eastern Goldfields Superterrane (EGST; Figure 1a), showing contrasting stratigraphy, age of metamorphism, seismic signature, and bulk crustal ages [Wyche *et al.*, 2012]. They are juxtaposed by the “Ida Fault,” a crustal-scale, E dipping shear zone that depending on the tectonic model has been interpreted as an intracratonic structure [Van Kranendonk *et al.*, 2013] or a major suture between allochthonous terranes [Myers, 1995]. This large-scale structure is truncated by the

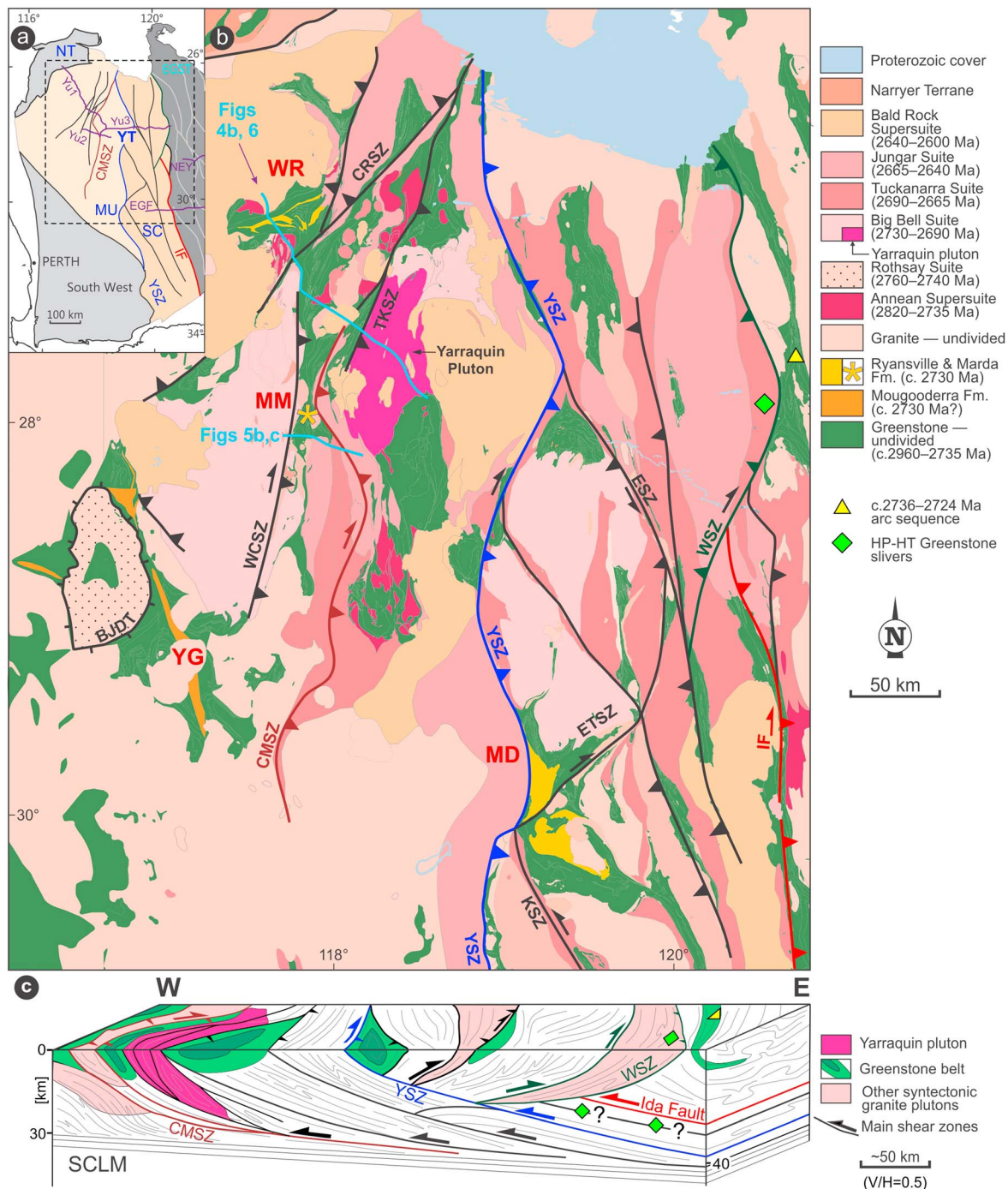


Figure 1. (a) Simplified map of the main geological subdivisions and shear zones of the western portion of the Yilgarn Craton, showing the main terranes and the network of craton-scale shear zones. EGST: Eastern Goldfields Superterrane; NT: Narryer Terrane. In the western half of the craton, the Youanmi Terrane (YT) is subdivided into Murchison (MU) and Southern Cross (SC) domains. Main shear zones are color-coded to facilitate their identification. IF: Ida Fault; YSZ: Youanmi Shear Zone; CMSZ: Cundimurra Shear Zone. The purple lines indicate the trace of the available seismic traverses: Youanmi traverses (Yu1–3): [Wyche *et al.*, 2013]; EGF: [Drummond *et al.*, 2000]; NEY: [Goleby *et al.*, 2004]. The rectangle shows the location of Figure 1b. (b) Interpreted geological map of the central portion of the Youanmi Terrane showing the location of the four greenstone belts preserving angular unconformities (MD: Marda-Diemals; MM: Mount Magnet; WR: Weld Range; YG: Yalgoo). The two light blue lines refer to the cross sections presented in this work. Abbreviations for the shear zones not shown in Figure 1a: CRSZ: Chunderloo Shear Zone; ETSZ: Edale Shear Zone; ETSZ: Evanston Shear Zone; KSZ: Koolyanobbing Shear Zone; TKSZ: Tuckabianna Shear Zone; WSZ: Waroonga Shear Zone; WCSZ: Wattle Creek Shear Zone; BJD: Badja Decollement. Map compilation is based on combined field and geophysical data. Locations of HP-HT greenstone slivers and the ~2736–2724 Ma arc sequence are from Zibra *et al.* [2017] and de Joux *et al.* [2014], respectively. (c) Block diagram summarizing the crustal architecture of the western portion of the Yilgarn Craton, as reconstructed by merging the results of the seismic traverses shown in Figure 1a. The Moho discontinuity and the highly reflective middle to lower crust are E dipping, overlying a seismically transparent subcontinental lithospheric mantle (SCLM).

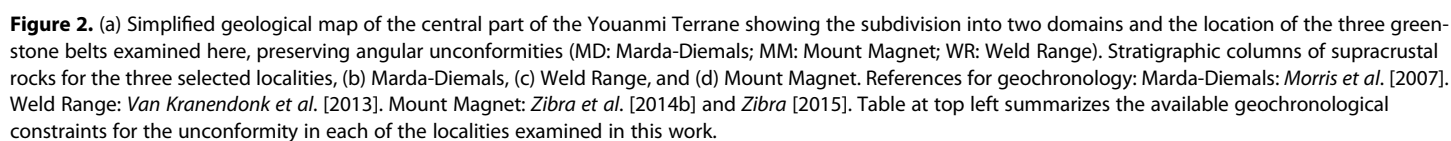
late-orogenic, W dipping Waroonga Shear Zone (WSZ, ~2660 Ma; Figures 1a–1c), which contains slivers of high-grade, Youanmi-type greenstones that were previously buried to lower crustal depths (Figures 1b and 1c) [Zibra *et al.*, 2017]. East of the Ida Fault, the main ~2730–2660 Ma EGST greenstone sequence [Hayman *et al.*, 2015], including an ~2736–2724 Ma arc sequence (Figures 1b and 1c) [de Joux *et al.*, 2014], is overlain by clastic sequences deposited above an ~2665–2655 Ma regional unconformity [Squire *et al.*, 2010]. West of the Ida Fault, the older Youanmi Terrane includes ~2960–2750 Ma greenstones dominated by mafic-ultramafic sequences interlayered with banded iron formations (BIFs), reflecting a prolonged period of lithospheric extension that accompanied the emplacement of asthenospheric magma [Van Kranendonk *et al.*, 2013]. Most Archean BIFs were chemically deposited in deep oceanic basins, and their geochemistry may record variable amounts of sedimentary input from volcanic ashes [Klein, 2005] and/or terrigenous detritus [Alexander *et al.*, 2008; Haugaard *et al.*, 2017]. The ~2810–2750 Ma BIFs of the Youanmi Terrane exhibit a trace element pattern marked by strong depletion in light rare earth element, Zr, Hf, K, Th, and U, a depletion trend that is more accentuated in the ~2750 Ma BIF of the Wilgie Mia Formation (Figure S1 and Table S1). These data indicate that these BIFs were deposited in a deep marine environment, away from major detrital input [Klein, 2005; Thurston *et al.*, 2012]. The stratigraphic record of the Yilgarn Craton shows a hiatus in the ~2950–2810 Ma time span [Wang *et al.*, 1998], and it is unclear whether this gap indicates the existence of a Mesoarchean unconformity (D₁ of Van Kranendonk *et al.* [2013, Figure 2]) or a paraconformity marking a period of tectonomagmatic quiescence. While minor granitic magmatism accompanied the development of the greenstone sequences since ~2810 Ma, crustal magmatic activity peaked in the ~2730–2600 Ma time span [Van Kranendonk *et al.*, 2013].

3. Unconformities in the Youanmi Terrane

In this section we summarize the available sedimentary, magmatic, and geochronological data that allow us constraining the geological setting in the Youanmi Terrane at the ~2730 Ma time slice. The ~2960–2750 Ma greenstones of the Youanmi Terrane are unconformably overlain by ~2730 Ma clastic sedimentary rocks associated with felsic volcanic rocks. These are the youngest sequences preserved in the terrane and belong to basins that were subsequently deformed and eroded; thus, our knowledge about their original extent and primary sedimentary features is necessarily incomplete. Clastic sedimentary rocks are now preserved in four distinct domains that are ~400 km apart (Figures 1 and 2): (i) in the Marda-Diemals greenstone belt (Southern Cross Domain), (ii) in the Weld Range greenstone belt (Murchison Domain), (iii) in the Mount Magnet greenstone belt (Murchison Domain), and (iv) in the Yalgoo greenstone belt (Murchison Domain), along the eastern margin of the Yalgoo dome (Mougooderra Formation [Zibra *et al.*, 2016]). Only the first three domains are treated here, given the current lack of tight geochronology constraints for the Mougooderra Formation. However, this formation unconformably overlies ~2800 Ma greenstones; it is lithologically similar and possibly coeval with the other siliciclastic formations examined here [Zibra *et al.*, 2016].

The best preserved clastic sedimentary rocks are exposed in two distinct sequences in the Marda-Diemals greenstone belt, in the hangingwall of the Youanmi Shear Zone, one of the crustal-scale, E dipping shear zones that crosscut the whole Yilgarn Craton (Figures 1, 2a, and 3). Here clastic rocks were deposited at ~2730 Ma in two adjacent, physically discrete basins [Morris *et al.*, 2007]. In the northern basin, the weakly deformed, >2 km thick Diemals Formation comprises a sedimentary sequence including conglomerate, sandstone, argillite, and shale and is preserved within a N-S trending-trending syncline (Figure 3). The Diemals Formation preserves intraformational unconformities and evidence of intraformational reworking, indicative of rapid deposition in an active tectonic setting [Chen *et al.*, 2003]. Geochemical data indicate that clastic material deposited in the lower part of the Diemals Formation was mainly sourced from the underlying ~3000–2800 Ma greenstones [Morris *et al.*, 2007]. The clastic material in these sediments becomes increasingly felsic up section, reflecting progressive exhumation and erosion of the greenstone substrate and the underlying granites [Morris *et al.*, 2007]. Clast lithology and the asymmetric distribution of facies in the lower part of the formation (Figure 2b) suggest that the clastic material was mainly sourced from the east [Wyche *et al.*, 2001; Morris *et al.*, 2007].

The Marda Complex comprises a sedimentary sequence at the base, similar to but coarser-grained than that in the Diemals Formation, with a conglomeratic base that contains similar populations of decimeter (dm)-sized clasts of proximal origin (Figure 2b). The similarities in the coarse-grained clastic component



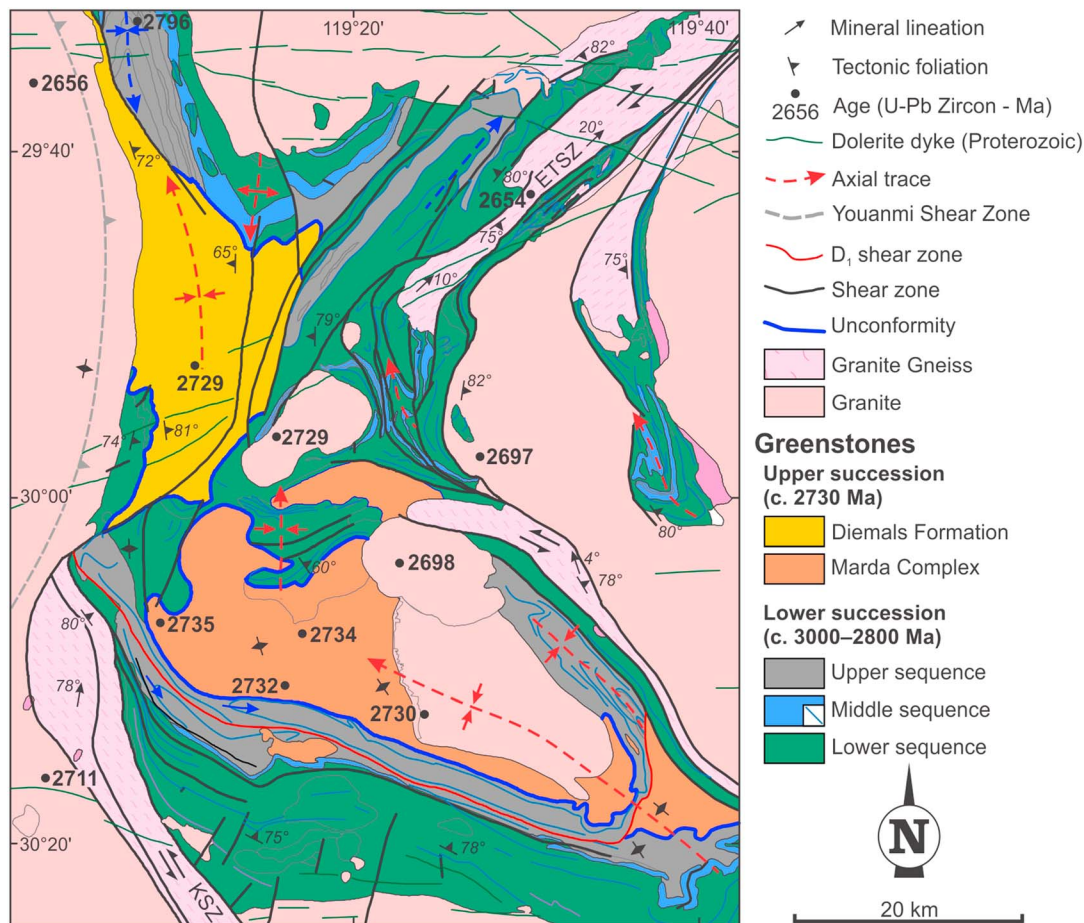


Figure 3. (a) Geological map of the Marda-Diimals greenstone belt. Redrawn after Wyche *et al.* [2001] and Riganti and Chen [2000]. Geochronology data after Morris *et al.* [2007]. Note that the shear zone assigned to D₁ postdates the ~2730 Ma Marda Complex.

suggest that the Diimals Formation is broadly coeval with the thick rhyolite packages that lay on top of the sedimentary sequence in the adjacent volcano-sedimentary Marda Complex [Morris and Kirkland, 2014]. A key difference in the Marda Complex is the presence of lenses of rhyolite and andesites (Figure 2b), overlain by interfingering lava flows, pyroclastic rocks, and minor volcanoclastic sediments that were erupted in a subaerial environment, with evidence of welding and rheomorphic flow in rhyolitic rocks [Wyche *et al.*, 2001]. Eruption took place during the deposition of proximal clastic sediments, derived from a source comparable with the underlying lower greenstone succession (Figure 2b) [Chen *et al.*, 2003]. The crystallization age of several volcanic members of the Marda Complex and their subvolcanic equivalents overlaps with the maximum depositional age for the Diimals Formation (2729 ± 9 Ma; Figure 2b [Morris *et al.*, 2007]).

In contrast to clastic formations in the Marda-Diimals greenstone belt, the Weld Range and Mount Magnet greenstone belts in the Murchison Domain are more deformed and therefore provide more fragmented information. The Weld Range greenstone belt (WR; Figures 2a and 2c and 4a and 4b) is sheared along the Cue Shear Zone Network, which is younger than ~2660 Ma (Figures 4a and 4b) [Zibra *et al.*, 2014b]. Here the stratigraphy below the unconformity includes gabbro and dolerite intruded into interlayered BIF and felsic volcanic rocks, with the latter having crystallization ages in the ~2752–2734 Ma time span (Figure 2c) [Van Kranendonk *et al.*, 2013]. Above the unconformity, the base of the siliciclastic Ryansville Formation is well preserved and includes boulder to pebble conglomerate mainly derived from the underlying BIF of the ~2750 Ma Wilgie Mia Formation [Van Kranendonk *et al.*, 2013, Figure 10]. The conglomerate is overlain by turbiditic sandstones in an overall fining-upward cycle, representing an ~1 km thick sequence deposited on alluvial fans, in turn overlain by ultramafic schists derived from komatiitic basalts and by thin felsic

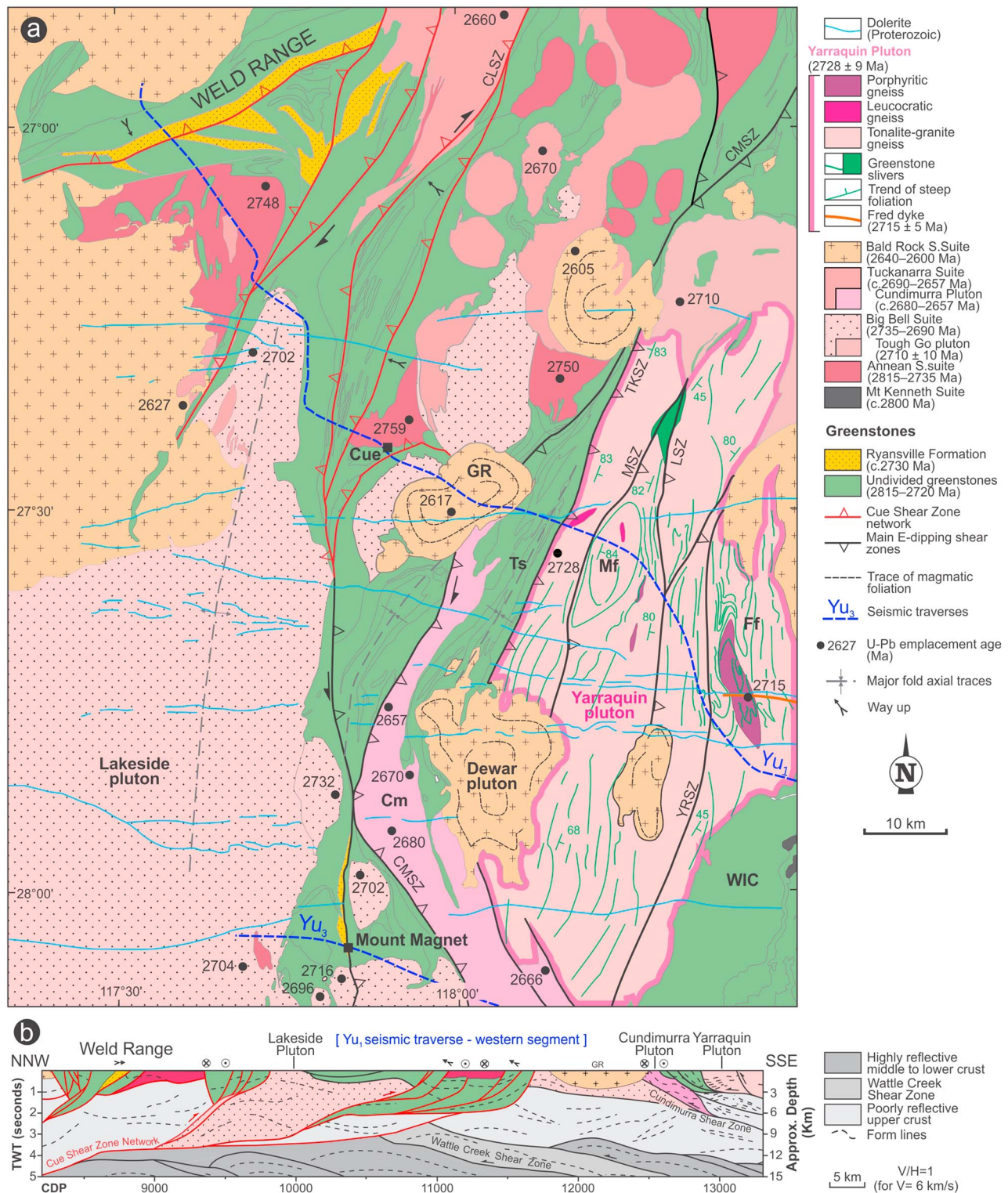


Figure 4. (a) Geological map of the central part of the Murchison Domain, centred on the three main N trending syntectonic plutons exposed in the area (from E to W: Yarraquin, Cundimurra (Cm) and Lakeside plutons). The dashed line labeled “Yu₁” represents the trace of the cross sections shown in Figures 4b and 7. Shear zones labels are as follows (from E to W): YRSZ: Yarloo; LSZ: Lake; MSZ: Mingimia; TKSZ: Tuckabianna; CMSZ: Cundimurra; CLSZ: Chunderloo. “Ts” indicates the Tuckabianna Syncline. “Mf” and “Ff” indicate Mingimia and Fred folds, respectively. “GR” indicates the Garden Rock Monzogranite. WIC indicates the Windimurra Igneous Complex. Geochronology data after Van Kranendonk *et al.* [2013] and Zibra *et al.* [2014a, 2014b]. (b) Geological cross section through the central part of the Murchison Domain, along the western portion of the seismic section Yu1. Greenstones in the Weld Range area are deformed by the ≤2660 Ma Cue Shear Zone Network. Redrawn after Wyche *et al.* [2013]. See Figures 1 and 2a for location.

volcanic units with a crystallization age of 2725 ± 4 Ma (Figure 2c). In this area, the age of the unconformity is therefore bracketed in the ~ 2734 – 2725 Ma time span (Figure 2c).

The pre-unconformity greenstone stratigraphy in the Mount Magnet area is largely comparable to that in the Weld Range area, with gabbro intruded into interlayered BIF and basalts of the Wilgie Mia Formation and with the latter postdating felsic volcanic rocks dated at 2748 ± 11 Ma (Figure 5a). The northern part of the belt, however, includes a thick sequence of mafic-ultramafic schists interlayered with BIF, predating the ~ 2800 Ma, BIF-bearing Yaloginda Formation. Marking the unconformity, the ~ 50 m thick conglomeratic base of the Ryansville Formation, equivalent to the one found in the Weld Range greenstone belt, discordantly overlies the Yaloginda Formation (Figures 2d and 5a–5c) and contains boulders and pebbles of chert, BIF, and mafic to ultramafic rocks derived from the underlying older sequence (Figure 6a). In this area, the ~ 250 m thick Ryansville Formation fines upward and includes grit, sandstone, and shale. It records three main folding events [Zibra *et al.*, 2014b], and it is cut by several generations of late-orogenic, NE trending shear zones (Figures 5a–5c) [Thompson *et al.*, 1990]. Felsic volcanic rocks, felsic tuffs, and agglomerates dated at 2727 ± 6 Ma [Schiotte and Campbell, 1996] are here interlayered with the Ryansville Formation and were locally erupted directly on BIF and cherts of the Yaloginda Formation (Figure 6b). Therefore, this volcanic age approximates the age of the unconformity in the Mount Magnet area.

In summary, a reassessment of the recent literature suggests that the clastic deposits preserved in the Youanmi Terrane share several first-order features and, in particular, (i) a base above an unconformity marked by conglomerates of proximal origin, derived from the underlying greenstones; (ii) dominant fining-upward turbiditic sequences in the upper portions of these formations; and (iii) felsic volcanic components and detrital zircons from clastic sedimentary rocks indicating that these basins formed roughly at the same time, at ~ 2730 Ma (Figure 2). We conclude therefore that the three greenstone belts considered here (Figure 2) contain clastic sediments that were deposited above a regional-scale (≥ 400 km), ~ 2730 Ma angular unconformity.

4. Neoproterozoic Structural Evolution in the Youanmi Terrane

Having established above that the three different clastic basins discussed here developed above a regional unconformity, this section reappraises the literature on the structural evolution of the Youanmi Terrane. We show that in the current literature, evidence for a regional deformation coeval with this unconformity is so far either lacking or ill-defined. Structural studies in the Yilgarn Craton have traditionally focussed on the highly mineralized EGST, where regional deformation started between ~ 2698 and 2681 Ma (D_1 [Cohalan *et al.*, 2015, and references therein]). Two major transpressional events, both reflecting bulk E-W shortening, developed in the ~ 2675 – 2657 Ma time span (D_2 ; during a period of widespread granite magmatism and conjugate strike-slip shear zones [Swager and Nelson, 1997; Weinberg *et al.*, 2003]) and before ~ 2635 Ma (D_3 [Chen *et al.*, 2001]).

In the less explored Youanmi Terrane, a pre- 2730 Ma D_1 event, possibly associated with thrusting, has been recognized in the Marda-Diemals area (Figure 3) [Chen *et al.*, 2003]. These authors proposed that D_1 is postdated by two deformation events, both reflecting E-W shortening, developed during the deposition of the Diemals Formation (D_2 , at ~ 2730 Ma) and during a major episode of granite magmatism (D_3 , at ~ 2680 Ma). We note, however, that Chen *et al.* [2003] did not provide either a statistically valid structural data set or shear sense indicators; therefore, the geometry and kinematics of the described structures are largely unknown. Moreover, structures regarded as D_1 thrusts and the N trending F_2 and F_3 folds affect both the Diemals Formation and the Marda Complex (Figure 3; see also Chen *et al.* [2003, Figures 2, 5, 6, and 11]), and therefore must be younger than ~ 2730 Ma. This view is corroborated by structural work south of the Marda-Diemals greenstone belt, which indicates that the regional D_1 fabric is younger than ~ 2691 Ma [Dalstra *et al.*, 1999]. Furthermore, it is not clear which criteria Chen *et al.* [2003] adopted to distinguish between D_2 and D_3 regional structures, which are both N trending and with steeply dipping axial surfaces. In our interpretation, the presence of map-scale refolded folds [Chen *et al.*, 2003, Figure 2] suggests that two major deformation events (D_1 and $D_2 + D_3$) recorded by Chen *et al.* [2003] in the central Youanmi Terrane must both be younger than ~ 2730 Ma.

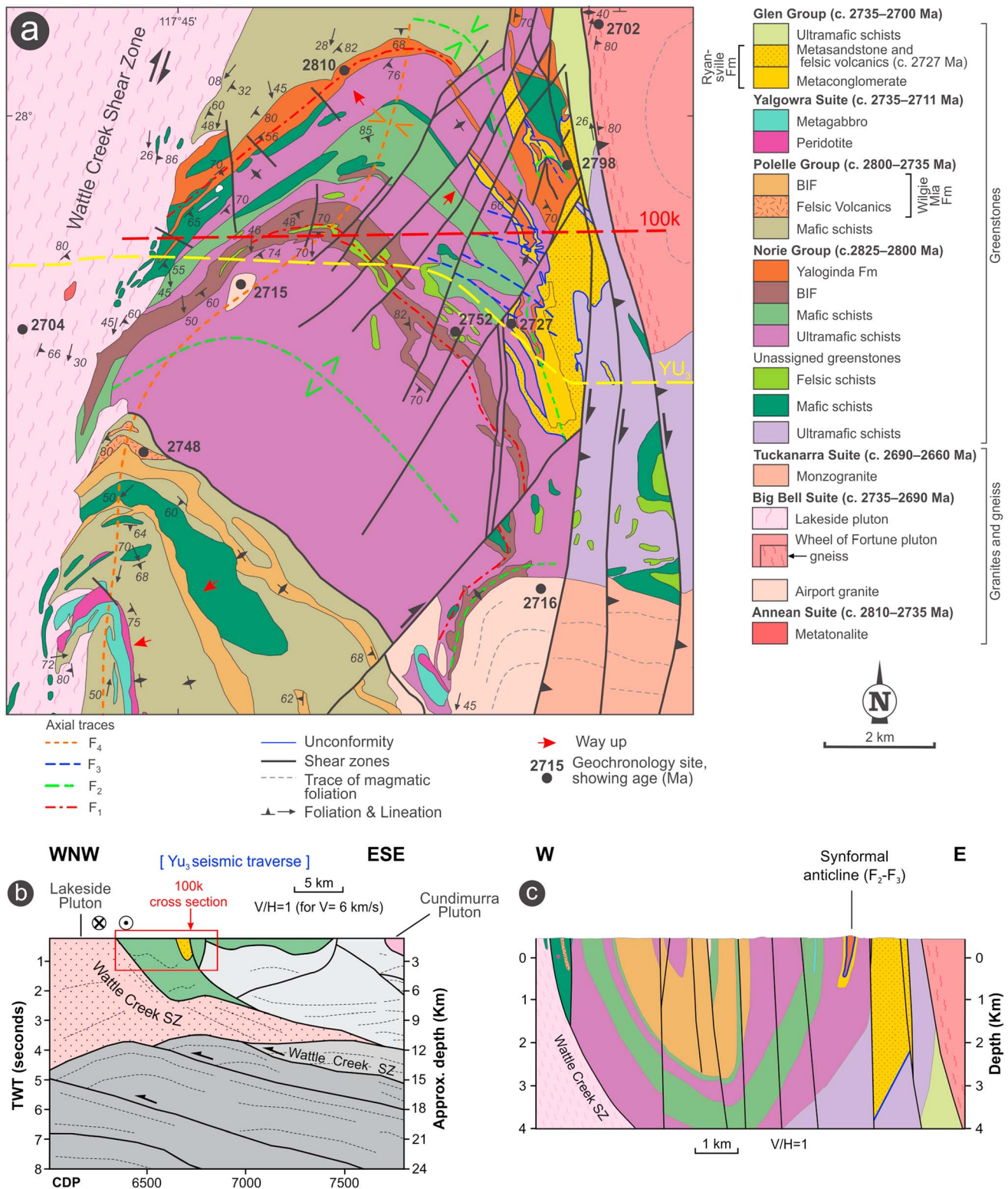


Figure 5. (a) Geological map of the Mount Magnet area, redrawn after Zibra [2015]. Geochronological data after Zibra *et al.* [2014a] and Zibra [2015]. Note that the ~2730 Ma unconformity is folded by the pre-~2704 Ma F_2 folds. (b and c) Geological cross sections through the Mount Magnet greenstone belt. Cross section derived from a combination of field data and interpretation of the western portion of the migrated seismic section Yu3 (Figure 5b). Structures within the greenstone belt are not easily recognizable in the seismic section. Redrawn after Zibra *et al.* [2014b]. This more detailed cross section shows the late F_4 synform, whose axial trace is subparallel to the Wattle Creek Shear Zone (Figure 5c). The cross section also intersects the synformal anticline refolding the unconformity. Redrawn after Zibra [2015]. See Figures 1 and 2a for location.

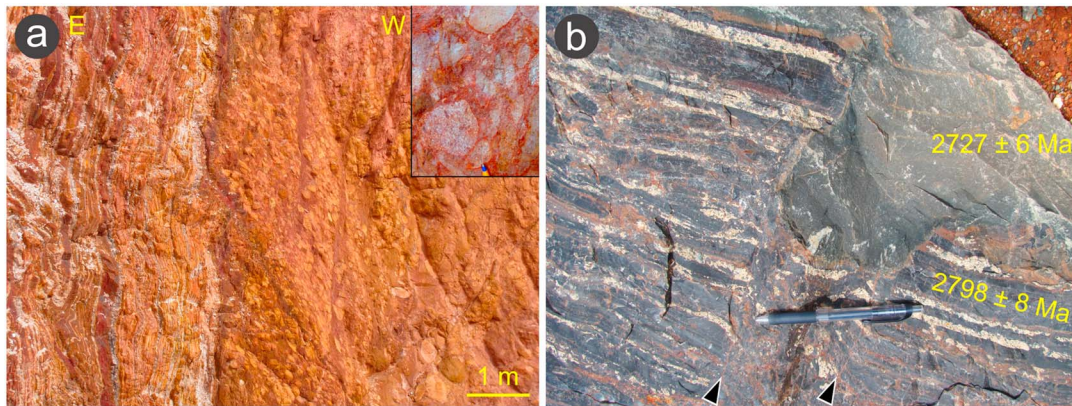


Figure 6. Outcrop-scale appearance of the regional unconformity in the Mount Magnet area. (a) Subvertical exposure showing the unconformable sedimentary contact between layered metachert (heteropic with the BIF) and the ~20 m thick conglomeratic base of the Ryansville Formation, which mainly contains rounded clasts of metabasalts and metachert. Inset at top right offers a close-up view of well-rounded clasts of porphyritic basalt (note white plagioclase phenocrysts) and aphanitic komatiitic basalt. (b) Exposed unconformity between the ~2798 Ma BIF and ~2727 Ma felsic volcanic rocks. The arrowheads point to meter-scale brittle shear zones that predated (or were contemporaneous with) the eruption of the felsic volcanic rock.

In the footwall of the Marda-Diemals greenstone belt, the Youanmi Shear Zone (YSZ in Figures 1 and 2a) is a craton-scale structure that juxtaposes the Murchison and the Southern Cross domains. The importance of this shear zone has already been stressed by *Gee et al.* [1981] and by *Myers* [1995, Figure 1], who recognized the contrasting stratigraphic evolution between the two adjacent domains. Therefore, it is likely that the Youanmi Shear Zone was formed already in the early stages of craton evolution. However, mainly because of younger tectonomagmatic overprint, the existence of pre-~2700 Ma deformation episodes along this shear zone has not been documented. In fact, the Youanmi Shear Zone was intruded by ~2711–2654 Ma granite plutons and was overprinted by the ≤ 2654 Evanston Shear Zone and by the Koolyanobbing Shear Zone (ESZ and KSZ, respectively; Figures 1b and 3), which were active in the ~2691–2650 Ma time span [*Qiu et al.*, 1999]. Accordingly, none of the structures exposed in the Southern Cross Domain show unambiguous evidence of a pre-2730 Ma activity.

In the Weld Range area of the Murchison Domain (Figure 2), the development of the ~2730 Ma unconformity has been assigned to the local D₂ event of unknown tectonic significance [*Van Kranendonk et al.*, 2013]. The bulk of the regional deformation in this area occurred later, during the sequential emplacement of the Lakeside and Cundimurra plutons at ~2700 Ma and 2680–2660 Ma, respectively (Figure 4a). These adjacent plutons were emplaced along large-scale, N trending and E dipping transpressional shear zones, during the development of a crustal-scale, E dipping pervasive magmatic to solid-state foliation (Figures 4b and 5b) [*Zibra et al.*, 2014a, 2014b]. Field and geophysical data show that these structures are postdated by the Cue Shear Zone Network, a system of localized and low-grade W dipping shear zones (Figures 4a and 4b) [*Zibra et al.*, 2014b], postdating the 2660 ± 3 Ma Chunderloo granite [*Van Kranendonk et al.*, 2013], which is sheared along the northern margin of the Cue network (Figure 4a).

The Mount Magnet greenstone belt recorded four main folding events, all postdating the ~2730 Ma unconformity (Figure 5a) [*Zibra et al.*, 2014b]. Here the unconformity is folded by large-scale isoclinal F₂ folds, which are in turn postdated by the ~2706 Ma Wattle Creek Shear Zone (Figure 5a) [*Zibra et al.*, 2014b]. F₂ isoclinal folds are refolded by upright F₃ folds, producing large-scale synformal anticlines cored by the ~2800 Ma chert and BIF of the Yaloginda Formation (Figure 5b). The N trending shear zones exposed along the eastern side of the belt developed at ~2680–2660 Ma, during the activity of the Cundimurra Shear Zone (Figures 5a and 5b), and are in turn postdated by a NE trending network of brittle shear zones (Figures 5a and 5c) that represent the youngest structures in the area.

In summary, a reappraisal of the recent literature shows that the main structures throughout the Yilgarn crust are roughly N trending and reflect several tectonomagmatic pulses associated with bulk E-W shortening that occurred in the 2700–2635 Ma time span. The main deformation events were broadly coeval over an ~500 km wide domain, referred to here as the Yilgarn Orogen [*Vearncombe*, 1998]. We note, however, that so far none of the orogenic Yilgarn structures can be unambiguously linked in space and time to the ~2730 Ma

deformation event that produced the regional unconformity. We show next that the Yarraquin pluton preserves evidence of this early event and helps timing the start of the orogeny.

5. The Yarraquin Pluton: Geological Setting and Geophysical Data

The following sections present geophysical and mesostructural to microstructural data from the Yarraquin pluton, exposed in central part of the Murchison Domain (Figures 1 and 4a). As detailed below, this pluton is roughly coeval with the ~2730 Ma regional unconformity and is pervasively deformed, offering therefore the chance to investigate structures that could potentially be coeval with the regional event of surface uplift recorded in the greenstone sequences (section 3).

The Yarraquin pluton is ~100 km long in the NNE-SSW direction and ~40 km wide (Figure 4a), bounded in the west by the ~2810 Ma host greenstone sequence in the east by the 2813 ± 3 Ma Windimurra Igneous Complex [Van Kranendonk *et al.*, 2013], and it is truncated by the Cundimurra Pluton in the SE. The Yarraquin pluton comprises mainly tonalite to granite gneiss interlayered with 5–200 m thick, up to 20 km long greenstone slivers that occur as NE trending linear belts. These slivers include amphibolite, micaschist, BIF, ultramafic schist, and quartzite. Along its northern margin, the Yarraquin pluton and its internal structures are cut by the undeformed 2710 ± 10 Ma Tough Go Monzogranite (Figure 4a) [Van Kranendonk *et al.*, 2013], while the eastern and the southwestern portions of the Yarraquin pluton are intruded by large posttectonic granites of the ~2640–2600 Ma Bald Rock Supersuite (Figure 4a; [Zibra *et al.*, 2013, 2014a]). The pluton contains four major shear zones, associated with two, kilometer-scale, N trending folds highlighted by elongate greenstone slivers, the Mingimbia and Fred folds (Figure 4a). Internal structures are truncated by the Fred dyke, an ~10 km long, 50 m wide, E trending granite dyke dated at 2715 ± 5 Ma (Figure 4a) [Lu *et al.*, 2016]. A metatonalite from the western margin of the Yarraquin pluton returned a magmatic crystallization age of 2728 ± 9 Ma [Wingate *et al.*, 2014]. Preliminary whole-rock geochemical data (Table S2) indicate that the Yarraquin pluton is composed of typical Archean high-Al TTGs (tonalite-trondhjemite-granodiorite), reflecting partial melting of a basaltic source composition at pressures ≥ 10 kbar, where the melt residuum contains garnet but not plagioclase [Champion and Smithies, 2007].

The seismic traverse YU1 intersects at high angle most of the main regional structures [Zibra *et al.*, 2013], offering good geometrical constraints for the study area (Figures 4a and 7). In cross section, major shear zones and fold axial surfaces are E dipping and show overall listric geometry. The pluton itself is imaged as a wedge-shaped, E dipping body, a feature that the Yarraquin pluton shares with the adjacent Lakeside and Cundimurra plutons (Figures 5b and 7) [Zibra *et al.*, 2014a, 2014b]. The four main E dipping listric shear zones that flank pluton (from west to east: Tuckabianna, Mingimbia, Lake, and Yarloo Shear Zones; Figure 8) merge at 12–15 km depth into a single surface, which is subparallel to the younger Cundimurra Shear Zone.

6. Yarraquin Pluton: Mesostructural Data

Within the Yarraquin pluton, we identify two structural domains: (i) the internal domain, showing magmatic to gneissic fabrics, and (ii) the mylonitic domain, on the western margin of the pluton (Figure 8). In both domains, granites show a subvertical, NE trending foliation, parallel to the regional fabric defined by the western pluton boundary, to the trace of the Tuckabianna Syncline, to the major internal shear zones, and to the long axes of greenstone slivers.

6.1. Internal Domain

The main foliation in granitic rocks (S_{HT}) ranges from magmatic to gneissic. Magmatic foliation is defined by the preferred orientation of euhedral K-feldspar and plagioclase phenocrysts, associated with nearly equidimensional quartz grains. Gneissic fabric mainly occurs along the three major internal shear zones. Gneisses in these domains show elongate quartz grains and rounded feldspar porphyroclasts wrapped by elongate biotite aggregates. These structural elements also mark a well-defined mineral and stretching lineation (L_{HT}). Gneissic fabric occurs along anastomosed networks of discrete, centimeter-thick high-strain zones, showing sharp to gradational boundaries with host magmatically foliated domains (Figures 9a and 9b). Gneissic fabric includes meter-scale shear zones centred along thin and discontinuous leucogranite veins, with linked arrays ranging from subparallel to perpendicular to the gneissic fabric (Figure 9c). They are

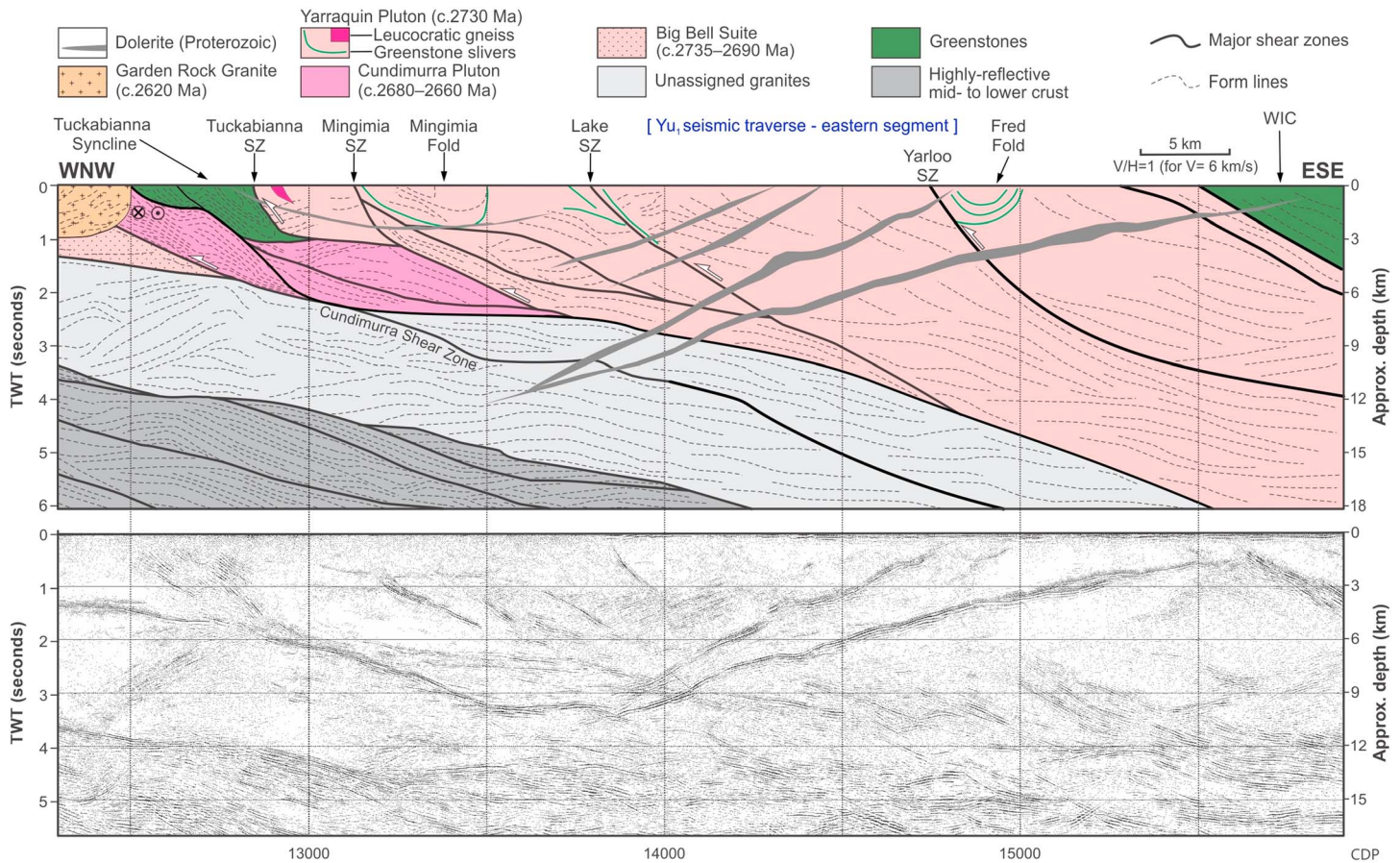


Figure 7. Migrated seismic section for the central segment of the seismic line Yu1, centred on the Yarraquin pluton, showing both interpreted and uninterpreted versions. Note that along the eastern portion of the Yarraquin pluton, the Yu1 line runs at $\sim 30^\circ$ to the internal fabric (Figure a), so structures in that area are likely steeper than imaged in the seismic section. The westernmost part of this section (cdp ~ 12500 – 13500) partially overlaps with the easternmost portion of the section shown in Figure 4b (note that the two sections have different scale). WIC indicates the Windimurra Igneous Complex. See Figures 1 and 2a for location

unfoliated to weakly foliated and show irregular, diffuse margins against host gneiss (Figure 9d). With the support of microstructural data (section 7), we interpret these veins as melt segregation structures (equivalent to set 2 and 4 segregation types of Sawyer [2000]). Within high-strain zones, both greenstones slivers and surrounding gneiss commonly show isoclinal folds with gently to steeply plunging axes (Figures 9e and 9f), which are invariably subparallel to the local trend of L_{HT} .

Throughout the pluton, greenstone slivers commonly contain coarse-grained SL tectonites, with finite strain (indicated by the intensity of S_{HT}) that markedly increases toward the main internal shear zones. Metasedimentary rocks commonly show completely transposed bedding, with centimeter- to plurimetric-sized isoclinal to sheath folds (Figure 9g). The more competent amphibolite slivers are commonly migmatitic, with segregation of centimeter-sized, clinopyroxene- or garnet-bearing tonalitic leucosomes (Figures 9h and 9i) that in places occur as boudin neck infill (Figure S2), testifying the melt-present nature of shearing.

6.2. Mylonitic Domain

In this domain, gneisses are SL tectonites displaying a well-developed NNE trending mylonitic foliation (S_{MYL}) highlighted by biotite flakes and elongate quartz ribbons, wrapping around sigmoidal feldspar porphyroclasts (Figures 10a and 10b). A prominent and steeply plunging stretching lineation (L_{MYL}) is marked by recrystallized quartz, feldspar, and biotite aggregates. Leucocratic veins commonly show isoclinal folds and boudinage, with fold axes subparallel to L_{MYL} (Figure 10a), suggesting high finite strain accumulated in highly ductile environment. In the western pluton aureole, amphibolites are steeply lineated SL tectonites that show no evidence of melt-present deformation, in striking contrast with what is commonly observed within the pluton (Figures 9h and 9i and S2). BIFs show three distinct generations of folds. Subvertical isoclinal and

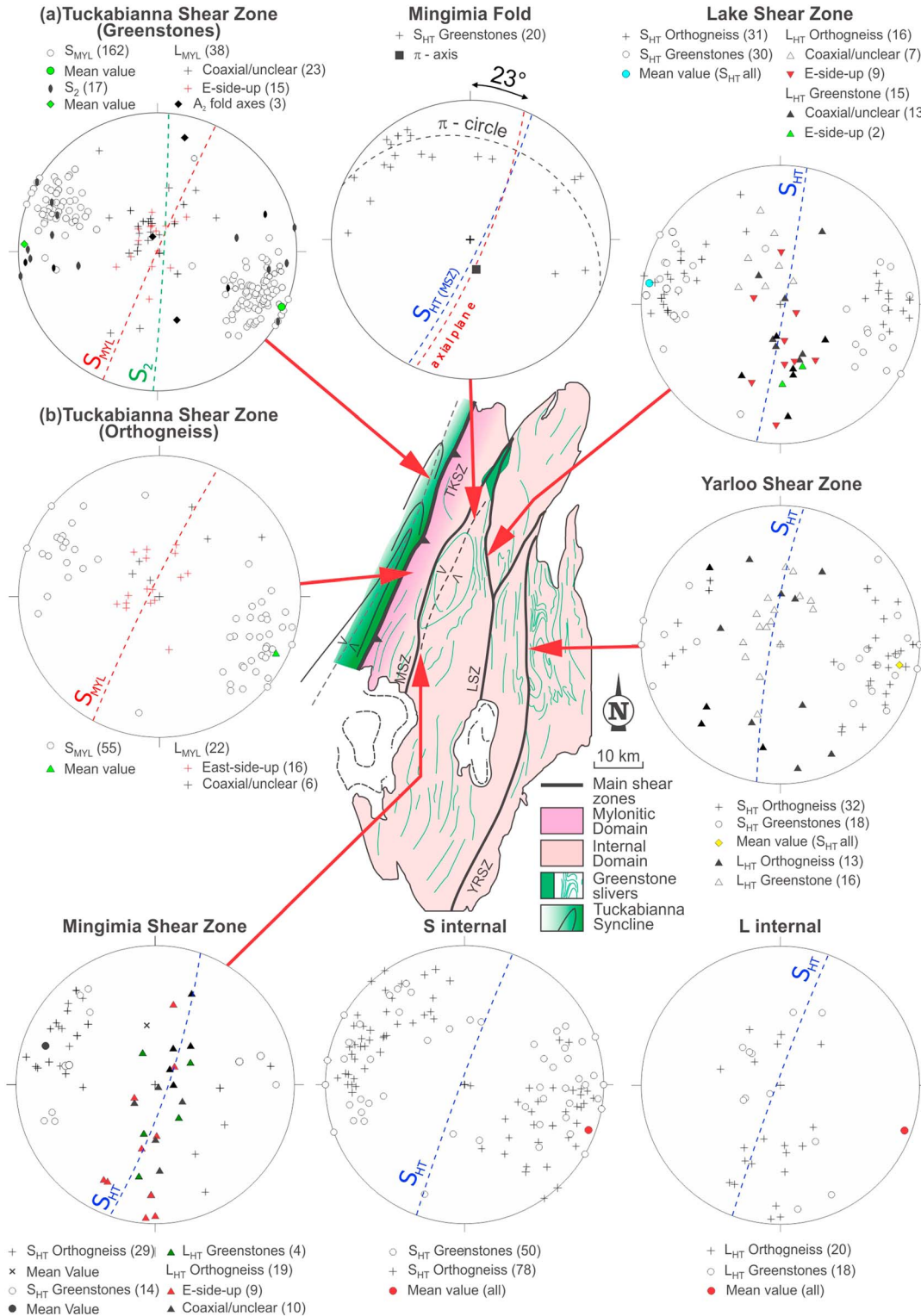


Figure 8. (a and b) Summary of structural data (foliation, lineation, and shear sense, on equal-area plots) collected for each structural domain identified within the Yarraquin pluton. The dashed lines indicate the planes corresponding to each mean value pole. Within the internal domain, we plotted together orientation data from magmatic and gneissic fabrics as S_{HT} and L_{HT} . These data are grouped in order to reflect the outcrop-scale gradual transition between gneissic and magmatic fabrics. Also, data from the main internal structures (labeled as “S internal” and “L internal”) are separated from those collected away from these structures. The axial plane of the Mingimnia Fold corresponds to the plane intersecting the π axis (i.e., the pole of the π circle) and the fold axial trace trending N 023° (red dashed line), as calculated on the geological map. This analysis shows that the main foliation of the Mingimnia Shear Zone ($S_{HT} (MSZ)$) is axial planar to the Mingimnia Fold.

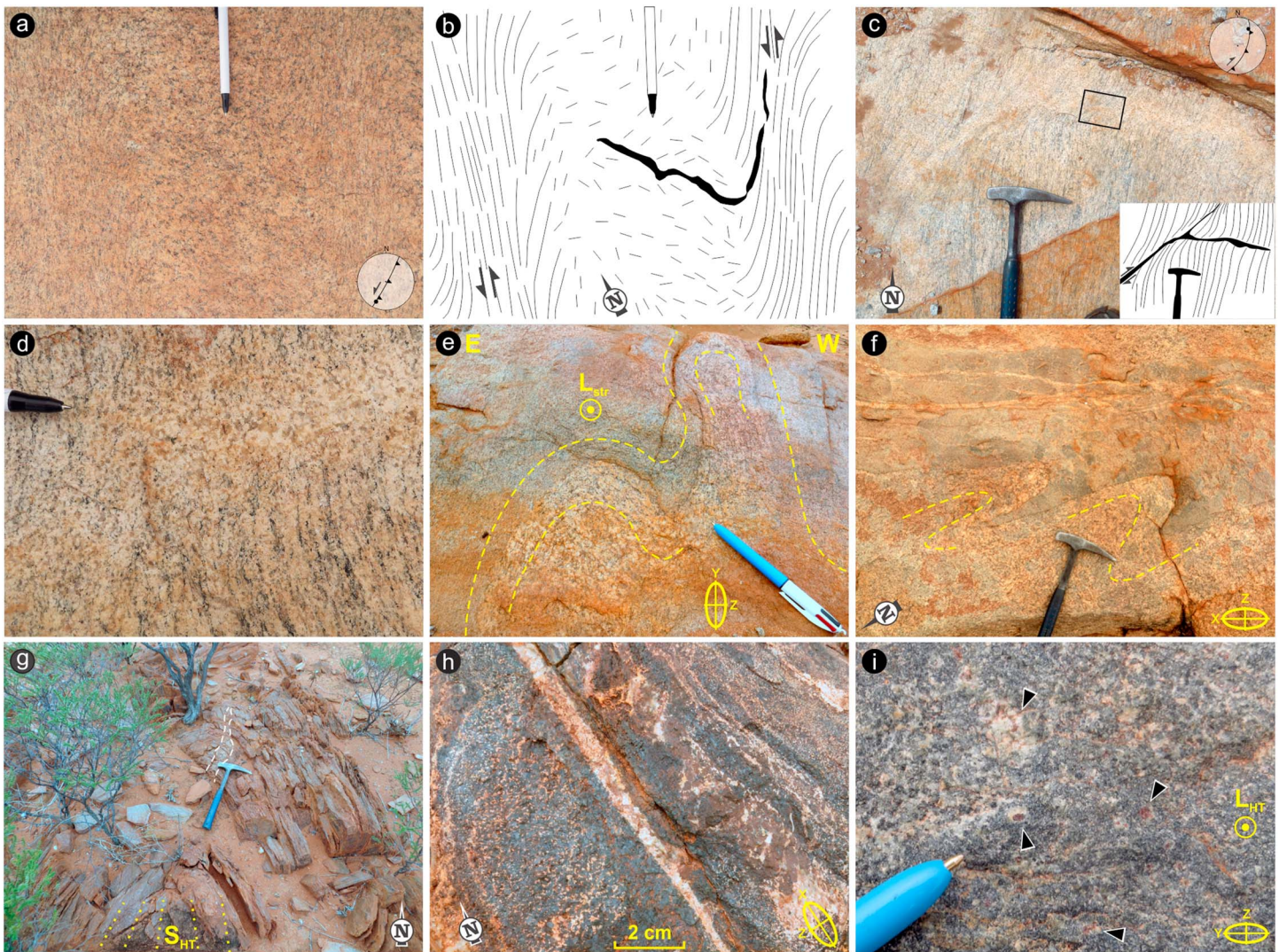


Figure 9. Representative outcrop-scale structures from the internal domain. (a) Flat-lying pavement showing two centimeter-thick, high-strain zones separated by a low-strain zone in tonalite gneiss exposed along the axial plane of the Mingimnia Fold. Since at this locality L_{HT} is moderately ($15\text{--}30^\circ$) S-plunging (see inset of equal-area plot), the sinistral shear sense visible in these horizontal exposures reflects top-to-W, oblique kinematics. (b) Line drawing of Figure 9a, highlighting the transition from the undeformed tonalite to the shear zones and the sigmoidal foliation pattern within the shear zones, which define the sinistral sense of shear. The black layer represents a folded and boudinaged quartz vein. (c) Flat-lying pavement showing high-strain fabric in tonalite gneiss, Lake Shear Zone. S_{HT} is sheared along narrow high-strain zones filled by leucogranite. Deflection of foliation indicate dextral shear sense. Note the stereonet inset showing the main foliation and lineation. The dextral shear sense visible in these horizontal exposures reflects top-to-W, oblique kinematics. The rectangle indicates the location of Figure 9d. (d) Close-up view of the shear zone in Figure 9c, at high-angle from S_{HT} . Note that leucogranite is undeformed and shows diffuse margins against host gneiss. (e) Subvertical exposure showing upright folds developed along the intrusive contact between a bluish microtonalite vein and host tonalite. The dashed lines highlight the trace of the folded S_{HT} . (f) Flat-lying portion of the outcrop shown in Figure 9e. The intersection between the subhorizontal surface and the upright folds with shallowly N plunging axes exposes synformal keels of microtonalite within host tonalite gneiss. The dashed lines highlight the trace of the folded S_{HT} . (g) Plurimetric tight fold showing steeply plunging axis (subparallel to L_{HT}) in micaschist, Yarloo Shear Zone. The yellow dashed lines highlight the prominent axial planar foliation (S_{HT}). The white dashed lines highlight a leucogranite vein intruded along the axial plane. (h) Detail of a migmatitic amphibolite sliver from the Lake Shear Zone, showing brown-weathered Cpx poikiloblasts within foliation-parallel tonalite leucosomes. (i) Detail from a migmatitic amphibolite showing mm-sized tonalite leucosome patches containing euhedral garnet grains and aggregates (arrowheads). Subvertical exposure nearly perpendicular to the subhorizontal L_{HT} .

sheath folds with steeply plunging axes subparallel to L_{MYL} (F_{1a} ; Figures 10c and 10d) are overprinted by isoclinal folds (F_{1b}) that are nearly coaxial and coplanar with the older folds, but showing a folded L_{MYL} and more rounded hinge zones. F_1 are locally refolded by N trending, upright, and parallel F_2 folds, associated with a spaced crenulation cleavage (S_2), which is better developed in schistose greenstone lithologies (Figure 10e). S_2 is recorded by the younger, largely undeformed intrusions (Fred dyke and Tough Go pluton; Figure 4a).

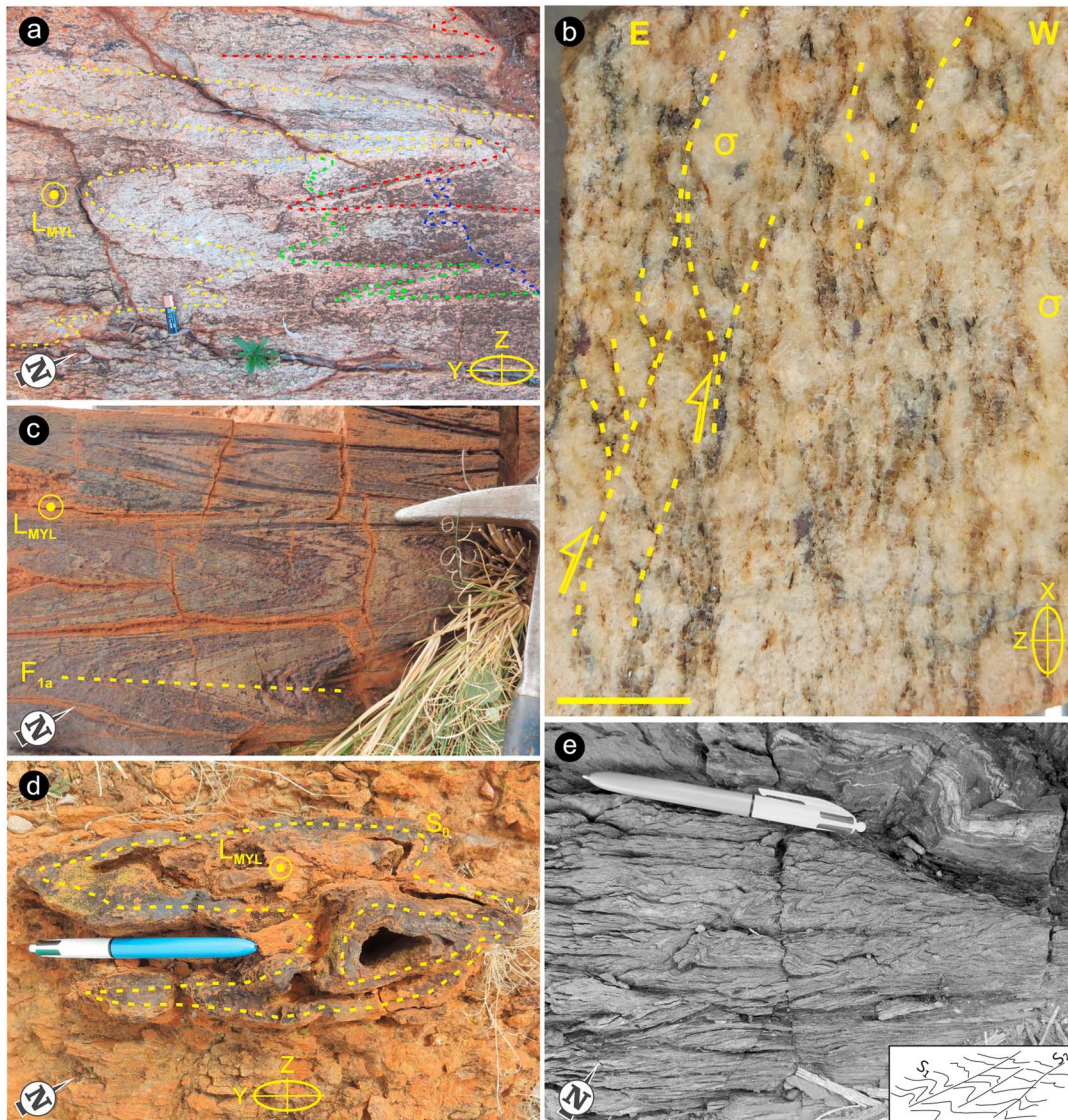


Figure 10. Typical outcrop-scale structures from the mylonitic domain (Tuckabianna Shear Zone) at the Western margin of the Yarraquin pluton. (a) Subhorizontal exposure of mylonitic tonalite, a few meters away from the contact with greenstones. Several generations of aplite and pegmatite veins are boudinaged and folded, with fold axes subparallel to L_{MYL} . (b) Polished sample from a subvertical exposure subparallel to L_{MYL} . Top-to-W sense of shear is indicated by prominent C' shear bands and sigma-type mantled plagioclase porphyroclasts (two examples indicated by " σ "). Scale bar is 1 cm. (c) Subhorizontal exposure showing isoclinal folds (F_{1a} ; the dashed line indicates the axial trace) in the ~2820 Ma BIF of the Norie Group. The steeply plunging fold axes are subparallel to L_{MYL} in both greenstones and adjacent granitic gneiss (compare with Figures 8a and 8b). (d) Subhorizontal exposure showing dm-scale sheath folds (F_1) in weathered BIF. The main axis (or nose) of the fold is subparallel to L_{MYL} in both greenstones and adjacent granitic gneiss. (e) Moderately pervasive, spaced and N trending crenulation cleavage (S_2) in layered felsic gneiss (likely a sheared volcanoclastic unit) near the western margin of the Tuckabianna Syncline.

6.3. Summary of Geometry and Kinematics

All the domains within the pluton share a comparable structural architecture represented by steeply dipping foliation and moderately to steeply plunging lineation (Figure 8). S_{HT} is commonly subvertical and N to NE trending in all lithologies, subparallel to the long axis of the pluton, to the internal shear zones and to the regional-scale greenstone lineament (Figures 1 and 4a). S_{HT} is also axial planar to the Mingimbia Fold (Figure 8). Likewise, the distribution of linear fabric is similar in all internal domains, with L_{HT} distributed along great circles subparallel to S_{HT} , reflecting along-strike variations in lineation plunge (Figure 8). S_{MYL} is essentially parallel to S_{HT} , while L_{MYL} is dominantly steeply plunging to subvertical (Figures 8a and 8b). The S_2 crenulation cleavage is N trending and subvertical, and it is therefore at low angle from S_{MYL} (~15° in strike difference; Figure 8a).

S-C and C' subfabrics, together with σ -type mantled porphyroclasts, indicate top-to-W, oblique kinematics in all the internal shear zones, regardless of the orientation of L_{HT} (Figures 8 and 9a–9c). Within the mylonitic domain, ~66% of the shear sense determinations, performed along the X-Z section of the finite strain ellipsoid, indicate top-to-W sense of shear (Figures 8, 10b, and S5), while the remaining ~33% suggest dominant orthorhombic symmetry.

7. Microstructures and Quartz Crystallographic Preferred Orientation

7.1. Internal Domain

At grain scale, there is no significant difference between the typical microstructure of tonalite samples collected along the main internal shear zones and the background magmatic to gneissic foliation preserved away from these structures. Samples from shear zones show stronger preferred orientation but no grain size reduction with respect to their magmatic precursor. Quartz-plagioclase boundaries in gneissic domains commonly show curved (cusate-lobate) outlines, and quartz shows chessboard subgrain boundary pattern [Kruhl, 1996], reflecting crystal-plastic deformation at near-solidus temperatures (diffusion and dislocation creep [Gower and Simpson, 1992; Zibra *et al.*, 2012]). However, the occurrence of euhedral to subhedral plagioclase phenocrysts (or aligned albite twin planes in anhedral plagioclase grains; Figure 11a), surrounded by anhedral quartz grains showing low aspect ratios, indicate that S_{HT} has a magmatic origin [Paterson *et al.*, 1989].

Tonalites sampled along the internal shear zones (Figures 9a–9f) show a peculiar, bimodal microstructure (Figures 11b and 11c). The coarse-grained plagioclase-quartz rock framework (average grain size >1 mm) shows deformation features comparable to those found away from the main shear zones, but the degree of modification of the primary magmatic fabric is generally more intense (Figure S3). Plagioclase-quartz boundaries are in fact more strongly curved, and quartz grains show more coarsely sutured grain boundaries, indicative of incipient grain boundary migration at high temperature [Stipp *et al.*, 2002]. On the X-Z section of the finite strain ellipsoid, the aspect ratio of quartz grains remains generally low (i.e., 1:1 to 3:1), so that quartz grains did not coalesce to develop ribbons (Figures 11a and S3). Therefore, even though in detail most quartz-feldspar grain boundaries show a variable degree of modification (cusate-lobate outlines), at the millimetre scale, the bulk of the magmatic framework is commonly preserved (Figure S3). Microscale shear sense indicators are generally absent, except for a coarse and irregular S/C fabric.

The coarse-grained tonalite framework contains 1–10 mm long microgranitic lenses (grain size: 10–200 μm), with equidimensional and randomly oriented albite-quartz symplectites (myrmekites) included by the late-magmatic, poikilitic K-feldspar. These lenses are preferentially situated within strain shadows and grain-scale fractures in larger plagioclase grains (Figures 11b and 11c and S3 and S4). In striking contrast with the tonalite framework, these granitic aggregates show pristine magmatic microstructures and little or no evidence of crystal-plastic deformation. In agreement with mesoscale evidence of melt segregation structures (Figures 9c and 9d), these aggregates likely represent small amounts of residual melt crystallized under stress, within low-pressure sites [Hibbard, 1987; Vernon, 2000]. Overall, these microstructures indicate that the myrmekites were produced during late-stage magmatic crystallization ([e.g., Phillips, 1974; Hibbard, 1987; Hopson and Rarnseyer, 1990] being texturally and genetically distinct from those resulting from deformation-induced replacement of K-feldspar [Simpson and Wintsch, 1989; Menegon *et al.*, 2006] or from contact metamorphism [Cesare *et al.*, 2002].

Slivers of migmatitic amphibolite (Figures 9h, 9i, and S2) commonly show a continuous foliation marked by granoblastic aggregates of elongate amphibole and plagioclase porphyroblasts. Thin films of quartz and plagioclase, containing rounded clinopyroxene grains, preferentially coat grain boundaries at high angle from S_{HT} (Figure 11d), indicating that these are former pockets of melt crystallized during deformation [Rosenberg and Riller, 2000; Sawyer, 2000]. Importantly, in both greenstone slivers and host tonalites, S_{HT} lacks any microstructural indication of moderate- to low-temperature overprint. There is neither evidence of brittle deformation and/or fine-grained, dynamic recrystallization in feldspar [e.g., Menegon *et al.*, 2008] nor undulose extinction and/or subgrain-rotation recrystallization in quartz [Stipp *et al.*, 2002], or hornblende and biotite replacement by actinolite and chlorite.

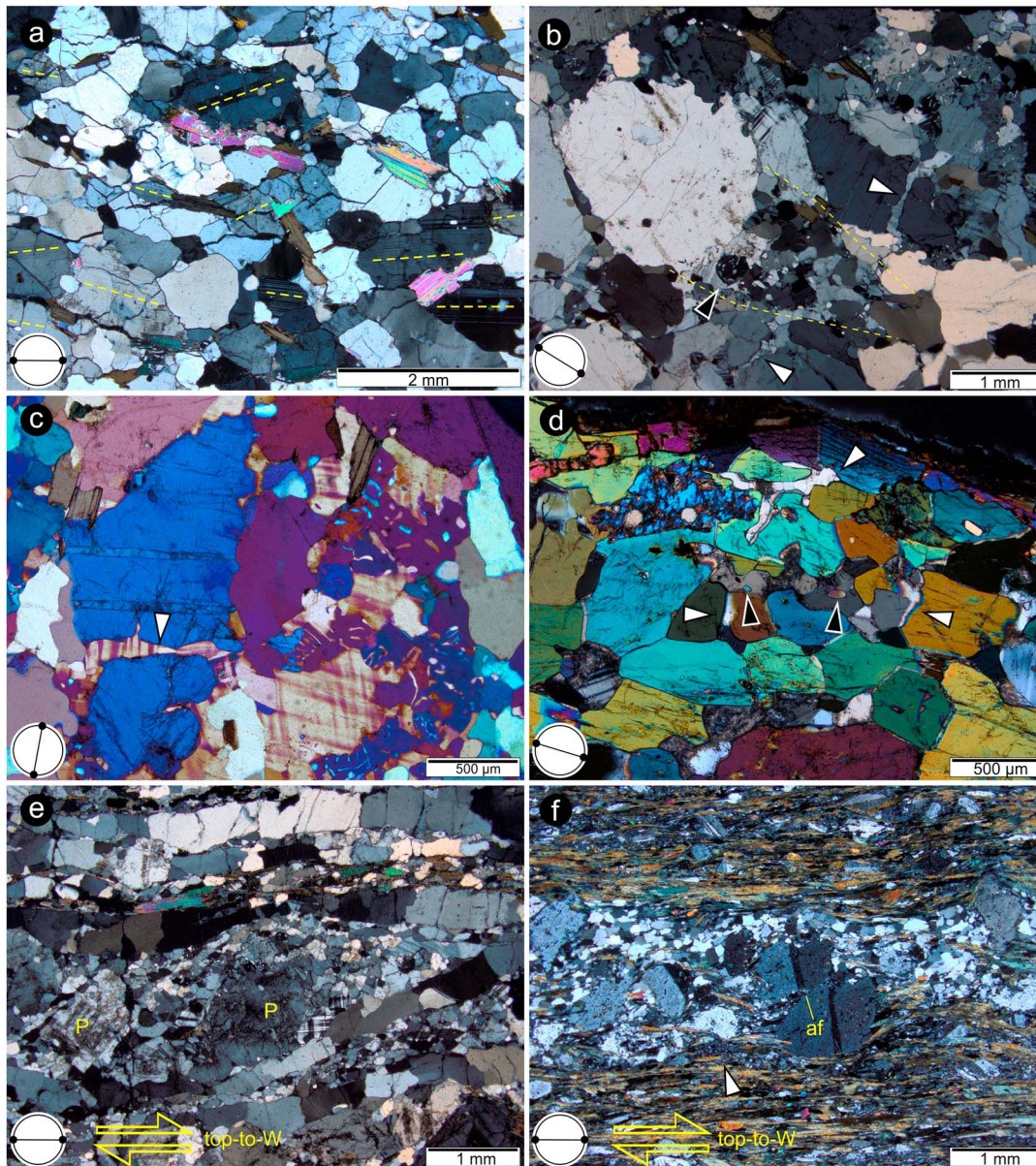


Figure 11. Chief microstructures from internal and mylonitic domains. Crossed polarized light. All thin sections were prepared perpendicular to foliation and parallel to lineation. (a) Magmatic foliation (S_{HT}) in tonalite from the internal domain. Subhedral to anhedral plagioclase phenocrysts show albite twins (yellow dashed lines) aligned with biotite and muscovite flakes. Note that most plagioclase-quartz phase boundaries show a cusped-lobate outline. Grain scale fractures are due to thin section preparation. (b) Typical microstructure from tonalite exposed along the internal shear zones. Sample 210250, from the outcrop shown in Figures 9c and 9d. Strain shadows around larger plagioclase grains contain fine-grained aggregates of granitic composition (outlined by yellow dashed lines) and typically include rounded albite-quartz myrmekites (black arrowhead). Plagioclase commonly shows magmatic microfractures healed by poikilitic K-feldspar (white arrowheads). (c) Close-up view of the top right corner of Figure 11b, rotated $\sim 70^\circ$ clockwise. An optically continuous, poikilitic K-feldspar grain encloses randomly oriented quartz, plagioclase, and myrmekites, postdating brittle deformation in plagioclase (arrowhead). Gypsum plate inserted. (d) Typical microstructure of migmatitic amphibolite slivers exposed along the internal shear zones (Figure 9h). Thin quartz and plagioclase films preferentially coat amphibole grain boundaries oriented at high angle to S_{HT} (white arrowheads) and show cusped shapes, whereas amphibole grains show rounded (corroded) outlines. Larger quartz-plagioclase lenses enclose rounded clinopyroxene grains (black arrowheads). (e) Typical microstructure of tonalite striped gneiss from the hanging wall of the Tuckabianna Shear Zone. S_{MYL} is defined by alternating layers of coarsely recrystallized plagioclase and straight, commonly one-grain-thick quartz ribbons. Note that the core of recrystallized feldspar aggregates contains plagioclase porphyroclasts showing remnants of oscillatory zoning ("P"), indicative of their magmatic origin. Top-to-W shear sense defined by sigmoidal quartz ribbons and σ -type mantled plagioclase porphyroclasts. (f) Mylonitic amphibolite from the footwall of the Tuckabianna Shear Zone. Aggregates of equidimensional quartz recrystallized grains and actinolite needles wrap around plagioclase porphyroclasts, which locally show antithetic microfault (af). Aggregates of recrystallized sodic plagioclase (arrowhead) are 10–50 μm in size. Top-to-W shear sense defined by S/C and C' subfabrics, σ -type mantled porphyroclasts and antithetic microfaults.

7.2. Mylonitic Domain

Tonalite exposed along the Tuckabianna Shear Zone are striped mylonitic gneisses. The typical microstructure includes straight, typically one-grain-thick polycrystalline quartz ribbons, separating quartz-poor layers of coarsely recrystallized plagioclase and K-feldspar (grain size: 100–500 μm), wrapping around remnants of large plagioclase porphyroclasts (Figures 11e and S5). Individual quartz grains are 300–500 μm thick, up to several millimetres in length, and show coarsely sutured grain boundaries (Figure S5). These microstructures typically occur in gneiss deformed at midamphibolite to granulite facies conditions ($T \gtrsim 600^\circ\text{C}$ [Hippert et al., 2001; Passchier and Trouw, 2005]).

In amphibolite from the shear zone footwall, plagioclase porphyroclasts show fracturing and are mantled by fine-grained ($\sim 10\text{--}30\ \mu\text{m}$) dynamically recrystallized grains of sodic plagioclase, while hornblende porphyroclasts are replaced by synkinematic actinolite and epidote (Figure 11f). Quartz forms polygonal aggregates of nearly equidimensional, recrystallized grains of fairly uniform grain size ($\sim 50\text{--}150\ \mu\text{m}$). These microstructures suggest that S_{MYL} in greenstones in the footwall of the Tuckabianna Shear Zone developed under lower amphibolite facies conditions [Stipp et al., 2002; Passchier and Trouw, 2005]. Further west, the NE trending axial planar foliation in mafic-ultramafic schists in the core of the Tuckabianna Syncline contains the synkinematic chlorite-actinolite \pm albite \pm quartz \pm talc assemblage, indicative of lower greenschist to midgreenschist facies conditions. These assemblages define S-C and C' subfabrics, and together with σ -type mantled plagioclase porphyroclasts, they invariably indicate top-to-W kinematics across the whole Tuckabianna Shear Zone (Figures 11e and 11f and S5).

7.3. Quartz Crystallographic Preferred Orientation

In order to constrain deformation temperature and prevailing shear sense in the domains identified within the Yarraquin pluton, we determined the quartz crystallographic preferred orientation (CPO) in 22 samples from micaschist and host tonalite (Figure 12). Additional data and details of the analytical method are provided in Table S2. Most samples from the internal shear zones show a dominant near-X maximum, in some cases associated with subordinate near-Z and near-Y maxima (Figure 12). Such fabric is indicative of dominant prism $\langle c \rangle$ slip in cooperation with subordinate prism and basal $\langle a \rangle$ slip and typically reflects dominant noncoaxial shearing at near-solidus temperatures, in the high-quartz field [Mainprice et al., 1986; Stipp et al., 2002; Zibra et al., 2012]. Three samples from the Yarloo Shear Zone showing more prominent near-Y (samples (e) and (u)) and near-Z (sample (r)) maxima do not exhibit any microstructural evidence of retrogression, suggesting the existence of a domainal fabric, as commonly observed in coarse-grained gneiss deformed at high temperature [Zibra et al., 2010]. Overall, our data show that there is no systematic variation in quartz CPO pattern between steeply lineated and shallowly lineated samples (Figure 12).

In sample 210250 (Figures 11b and 11c and S3 and S4), the CPO pattern of the large, deformed quartz grains (plot (1)) shows a prominent near-X maximum, reflecting dominant prism $\langle c \rangle$ slip during tonalite crystallization. In contrast, the fine-grained quartz population from the microgranitic lenses is undeformed and shows no shape fabric (Figures 11b and 11c and S4). Therefore, the strong CPO in these domains, with a prominent near-X maximum (plot (2)), likely reflects oriented grain growth with $\langle c \rangle$ axis subparallel to the main extension direction [Gapais and Barbarin, 1986; Zibra et al., 2012], during the very last stages of tonalite crystallization.

External symmetry (with respect to S_{HT} and L_{HT}) indicates top-to-W shear sense in 13 samples. However, only in four samples the shear sense is corroborated by mesoscale and microscale kinematic indicators (Table S2). This might reflect the fact that at high temperature, macroscopic kinematic indicators may be rare or absent [Passchier and Coelho, 2006], while a clear quartz CPO may develop, even at relatively low finite strain, through combined $\langle c \rangle$ slip and oriented grain growth.

Between the three samples of mylonitic gneiss from the Tuckabianna Shear Zone (Figures 11e and S5), sample (h) shows a prominent near-X maximum, associated with a weak near-Y maximum that as for the identical high-temperature fabric that prevails in the internal domain (Figure 12) reflects dislocation creep with dominant $\langle c \rangle$ slip and subordinate prism $\langle a \rangle$ slip [Stipp et al., 2002]. Samples (a) and (j) show a prominent near-Y maximum that in sample (a) is associated with a subsidiary near-Z maximum. The fabric in these samples is due to dominant prism $\langle a \rangle$ slip [Schmid and Casey, 1986] and, in agreement with the observed microstructures, reflects deformation in the low quartz field, at temperature in excess of $\sim 500^\circ\text{C}$ [Stipp et al., 2002; Zibra

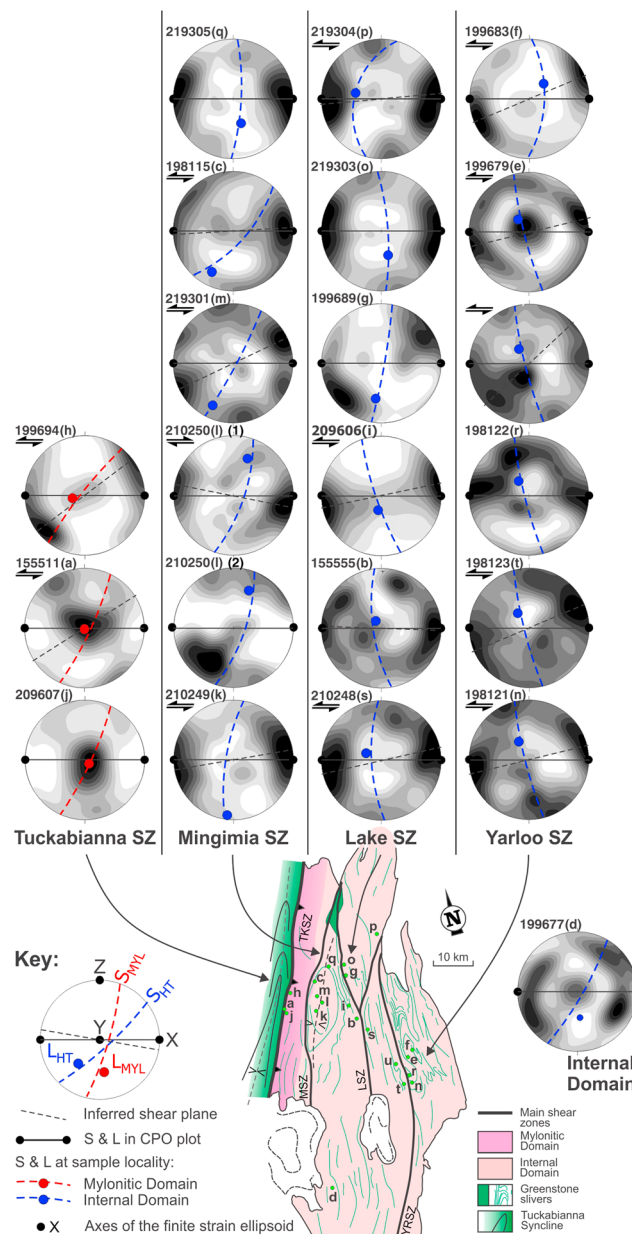


Figure 12. Summary of quartz CPO data from the Internal and mylonitic domains (equal-area stereographic projection lower hemisphere, 1% of search area, multiple uniform distribution). Additional information for each sample is provided in Table S2. Quartz CPO data are conventionally plotted in the sample reference frame characterized by E-W trending, vertical foliation, and by horizontal stretching or mineral lineation. The foliation is inferred to approximate the X-Y plane of the finite strain ellipsoid (with the X axis parallel to the lineation). Superimposed on the CPO pattern, the blue and red great circles and lines indicate the local orientation of foliation and lineation at the sampling site, respectively, for both the Internal and mylonitic domains. Further explanation is provided in the bottom left corner of the figure. Where possible, the orientation of the shear plane was inferred from the CPO pattern. For clarity, in the map showing sample locations, six-digit GSWA sample numbers are replaced by letters a–u, which are also reported near the corresponding plot, and in Table S2. For sample 210250, plot (1) refers to large quartz porphyroclasts forming the tonalite skeleton, while plot (2) refers to quartz grains measured in the microgranitic lenses located in strain shadow position (e.g., Figure 11b).

et al., 2012]. Assuming pluton emplacement at midcrustal levels (i.e., 3–5 kbar), maximum temperatures during solid-state shearing might have been in the order of ~650–700°C [Kruhl, 1996, Figure 3].

8. Discussion and Conclusions

8.1. The ~2730 Ma Regional Unconformity

The geological record preserved in greenstones indicates that in the ~2960–2750 Ma period, the Yilgarn crust was located in a deep basinal setting that allowed accumulation of a thick sequence of mafic-ultramafic rocks interlayered with BIFs. The complete absence of detrital input in BIF (Figure S1 and Table S1), a rock type that—because accumulated at very low depositional rates—is very sensitive to detrital input [Thurston *et al.*, 2012], suggests that such greenstone sequence developed far away from any emerged landmass, likely during a protracted period of dominant lithospheric extension that accompanied the emplacement of large volumes of mantle-derived magma [Van Kranendonk *et al.*, 2013].

The ~2730 Ma time slice evidently marks a regional-scale radical change in depositional setting (Figure 2), with the development of a regional unconformity and with the first occurrence of important detrital components of proximal origin (e.g., conglomerates at the base of the Marda, Diemals, and Ryansville Formations [Chen *et al.*, 2003; Morris *et al.*, 2007; Van Kranendonk *et al.*, 2013; Zibra *et al.*, 2014b]), derived from the erosion of the older greenstone sequence, and volcanic rocks locally erupted in subaerial conditions [Wyche *et al.*, 2001]. The record preserved in the Murchison Domain is particularly instructive, indicating that the deep-marine BIFs of the ~2750 Ma Wilgie Mia Formation were exhumed and eroded in the ~2734–2725 Ma time span during

which the unconformity developed (Figure 2). Such regional tectonostratigraphic evolution suggests the occurrence of an important, large-scale event of rock uplift. However, none of the structures known so far (section 4) could be unambiguously linked to such an early deformation event. We argue below that 2728 ± 9 Ma Yarraquin pluton and its structural record can do precisely that.

8.2. Syntectonic Emplacement of the Yarraquin Pluton

In the Yarraquin pluton, S_{HT} shows a consistent orientation, with N to NNE trending steeply dipping foliations prevailing in both the internal and the mylonitic domains (Figures 8 and 12a). L_{HT} shows along-strike variations in plunge (Figures 8 and 13c), but, regardless of its orientation, it is commonly associated with top-to-W kinematics (Figure 13a). The main fabric in granitic rocks of the internal domain ranges from magmatic to a concordant, high-temperature gneissic fabric (S_{HT}), with the latter prevailing along the main internal shear zones. Mesosstructure (Figures 9c and 9d) and microstructure (Figures 11a–11c and S3–S4), together with quartz CPO pattern (Figure 12), indicate that both fabrics developed at near-solidus temperature, in the high-quartz field, mostly under melt-bearing conditions, and therefore during pluton crystallization. The main fabric in greenstone slivers, concordant with that of enclosing granites, also developed in the presence of melt (Figures 9h and 9i, 11d, and S2). The nearly complete preservation of quartz CPO patterns indicative of dominant $\langle c \rangle$ slip (Figure 12) indicates that the retrograde overprint is negligible, given that this fabric can be easily overprinted by lower temperature fabrics, even in cases of small increments of retrograde finite strain [Blumenfeld *et al.*, 1986]. The Lake Shear Zone (LSZ; Figure 4a) provides the best example of synemplacement deformation under hypersolidus conditions, including melt segregation structures and migmatitic greenstone slivers (Figures 9c, 9d, 9h, and 9i and S2), together with microstructural evidence of crystallization of residual melt under stress (Figures 11b–11d and S4a and S4b). Overall, given the very limited postemplacement overprint (S_2), these structures reflect an important phase of synemplacement, E-W horizontal shortening (Figure 13).

In the mylonitic domain, the overprint of S_{HT} by S_{MYL} is associated with a drastic change in both mesosstructure and microstructure, with the appearance of high-temperature mylonitic fabric associated with widespread dynamic recrystallization (Figures 10b, 11e, 13b, and S5). Microstructures and quartz CPO patterns indicate that S_{MYL} developed at $T \gtrsim 500^\circ\text{C}$ (section 7), locally preserving evidence of shearing at near-solidus temperatures (Figure 12, sample (h)). Greenstones in the footwall of the Tuckabianna Shear Zone show an inverted metamorphic gradient, with microstructures indicating lower amphibolite facies conditions near the contact with the Yarraquin pluton, decreasing away from the contact down to lower greenschist to midgreenschist facies conditions in the core of the Tuckabianna Syncline (Figure 13). These data, together with the complete kinematic coupling between the pluton and host greenstones, suggest that the high-temperature mylonitic fabric preserved along the pluton margin developed during the late stages of pluton emplacement and necessarily before the emplacement of the undeformed ~ 2715 Ma Fred dyke and ~ 2710 Ma Tough Go pluton (Figure 4a).

Since the internal domain exhibits a single fabric developed at near-solidus temperature, it is likely that L_{HT} with along-strike variable plunge formed concurrently throughout the pluton. The coexistence of both gently and steeply plunging lineations along a structurally continuous shear zone is typical of transpressional systems and may reflect along-strike gradients in accumulated finite strain [Tikoff and Greene, 1997]. In this model, the coaxial pure shear component of deformation would have induced a switch in lineation orientation (from subhorizontal to subvertical), while the simple shear component would have produced fabrics with monoclinic symmetry on horizontal surfaces [Tikoff and Greene, 1997]. However, this kinematic model does not account for the structural evolution recorded by the Yarraquin pluton, given that domains characterized by subvertical stretching lineation, like the Tuckabianna Shear Zone along the pluton margin, exhibit a dominant component of noncoaxial deformation in sections parallel to the down-dip L_{MYL} (Figures 10b, 11e and 11f, and S5). Likewise, it is also unlikely that the lineation pattern simply reflects bulk flattening, given the well-clustered lineation data observed within the mylonitic domain, along the pluton margin (Figure 13c).

We propose an alternative interpretation, based on the fact that that shallow plunging L_{HT} in orthogneiss preferentially occurs in domains showing (mesoscale and/or microscale) evidence of melt-present deformation (Figures 9b and 9c and 12b–12d), whereas down-dip lineations occur in domains showing solid-state deformation. This suggests that strain partitioning during bulk transpressional deformation might have

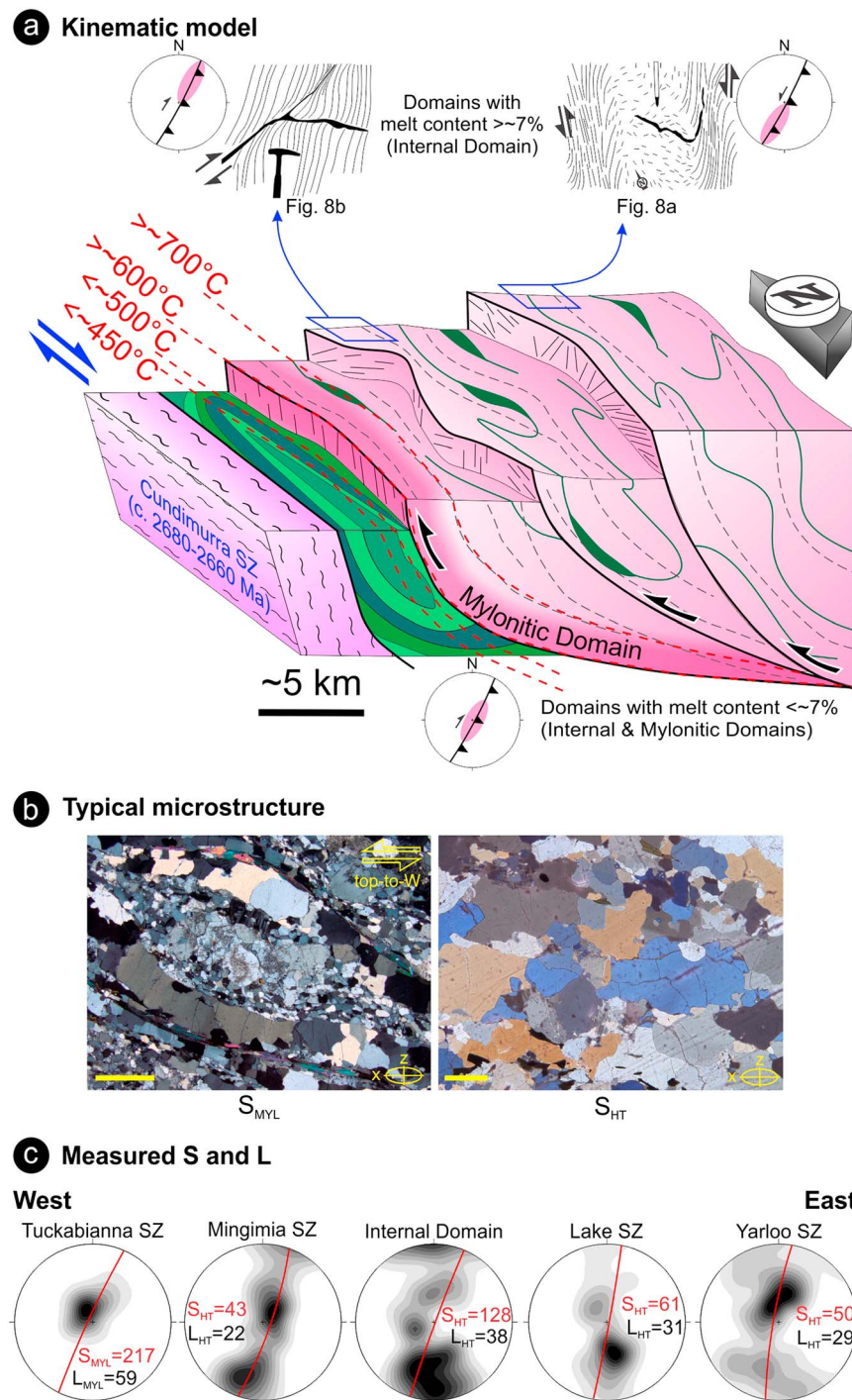


Figure 13. Conceptual model for the development of the pattern of mineral and stretching lineation during the emplacement of the Yarraquin pluton. (a) Schematic cross section through the western pluton boundary. Temperature estimation for metamorphic isotherms is based on microstructural data (section 7). All high-strain zones show a component of top-to-W kinematics. Outcrops showing evidence of melt-present shearing (internal domain) are generally associated with shallow-plunging lineation, with both dextral and sinistral shear components. In contrast, outcrops with no evidence of melt-present shearing (from both Internal and mylonitic domains) are mainly associated with steeply plunging linear fabric and top-to-W shear sense. Equal-area projection plots schematically illustrate (in pink) the position of the dominant lineations for each case. $\lambda/4$ retarder plate inserted. Left: Typical microstructure of coarse-grained gneissic foliation (S_{HT}) in tonalite from the internal domain. Right: Typical microstructure of mylonitic foliation (S_{MYL}) from the mylonitic domain. In both micrographs, the scale bar is 1 mm long. (c) Bulk orientation of mean foliation and distribution of lineation from greenstones and granitic gneiss, for each structural domain of the Yarraquin pluton.

produced the observed variability in L_{HT} orientation. In fact, during syndeformational pluton crystallization, we expect the occurrence of transient, and drastic, spatial, and temporal variations in viscosity, as a highly nonlinear function of decreasing melt content, particularly when crossing the rheological threshold of ~7% melt [Rosenberg and Handy, 2005]. If such a two-phase system is subjected to three-dimensional general shear, then strain partitioning is expected to occur at a variety of scale, from grain to lithospheric scale [Goodwin and Tikoff, 2002]. Under such conditions, melt-bearing, low-viscosity domains will localize the strike-slip component of shearing, while the more competent melt-free (or with $\leq 7\%$ melt content) domains will localize the dip-slip and coaxial components of deformation [Vigneresse and Tikoff, 1999]. In the case of the Yarraquin pluton, the distribution of L_{HT} on the foliation plane (Figure 13c) might therefore reflect strain partitioning related to heterogeneous spatial distribution of melt and therefore rock strength. Both S_{HT} and L_{HT} show similar patterns in orthogneiss and greenstone slivers, in agreement with the occurrence of both melt-bearing and melt-free structures in these rock types. In contrast, the Tuckabianna Shear Zone (in the mylonitic domain) shows top-to-W kinematics but no strike-slip components (Figures 8 and 13b and 13c), consistent with the subsolidus character of this shear zone (Figures 10a–10e, 11e and 11f, and S5). Given that the structures associated with the Yarraquin pluton reflect the coexistence of strike-parallel and dip-parallel, simple shear deformation (Figure 13), the bulk kinematics of the shear zone network associated with pluton emplacement likely reflects inclined transpression [Jones *et al.*, 2004].

In the seismic profile, all the main structures are listric and E dipping (Figure 7) but are subvertical to locally W dipping at the current exposure level (Figure 8). The geometry visible in the field likely results from the combined effect of (i) overall listric geometry of main structures in the area (Figures 4b, 5b, and 7) and (ii) steepening of the existing structures induced by a younger event of E-W horizontal shortening (D_2), which produced the subvertical crenulation cleavage (S_2). It is likely that the local D_2 deformation event occurred in the ~2680–2660 Ma time span, during the peak of tectonic activity along the adjacent Cundimurra Shear Zone (Figures 4a and 7) [Zibra *et al.*, 2014a]. Importantly, our mesostructural and microstructural data indicate that the D_2 fabric did not pervasively overprint the earlier S_{HT} and S_{MYL} fabric related to the emplacement of the Yarraquin pluton.

8.3. The ~2730 Ma Onset of the Neoproterozoic Yilgarn Orogeny and Implications for Archean Tectonics

The geological record preserved in the Yilgarn greenstones reflects an ~2730 Ma change in depositional setting, from an ~200 Myr long period of deep marine, low-energy environment to shallow marine and subaerial, high-energy conditions (Figure 14). Such dramatic switch suggests the inception of a regional scale orogenic event. We found that the tectonic signature of this event is recorded by the Yarraquin pluton, emplaced at 2728 ± 9 Ma along a network of large-scale, E dipping shear zones (Figure 7), reflecting a significant episode of synemplacement E-W shortening (Figures 13a and 14b). The 2750–2730 Ma time span includes the transition from distal marine sedimentation to the ~2730 Ma shallow-marine proximal clastic deposits and subaerial volcanic rocks and reflects the onset of the crustal shortening and thickening related to the Neoproterozoic Yilgarn Orogeny. The tectonomagmatic evolution of the ~2730 Ma Yarraquin pluton is interpreted as a record of this earliest process (Figure 14). The 2810–2750 Ma preorogenic granitic magmatism in the Yilgarn crust reflects melting of various crustal sources at a variety of pressures [Ivanic *et al.*, 2012], possibly induced by the progressive propagation through the crust of the same ~2815 Ma thermal anomaly that produced the greenstone sequence [Campbell and Hill, 1988; Van Kranendonk *et al.*, 2013]. In contrast, the Yarraquin pluton shows a clear TTG affinity (Table S2), reflecting partial melting of a mafic source localized at the base of a thickened crust [Champion and Sheraton, 1997; Martin *et al.*, 2005; Johnson *et al.*, 2017]. This change in granite chemistry may therefore result from the crustal thickening induced by the geodynamic switch that occurred in the ~2750–2730 Ma time span (Figure 14).

It is likely that at least part of the network of E dipping, crustal-scale shear zones that characterize the whole Yilgarn Orogen (Figure 1c) [Wilde *et al.*, 1996; Drummond *et al.*, 2000; Zibra *et al.*, 2014b] started to develop during the emplacement of the Yarraquin pluton given that in the study area, these large-scale structures seem to record negligible postemplacement modifications (Figure 8). Moreover, it is possible that such first-order structural architecture was inherited from the preorogenic stages of lithospheric extension (Figure 14a) associated with the development of the supracrustal sequences [Van Kranendonk *et al.*, 2013]. Some of the large-scale and long-lived Yilgarn structures, such as the Youanmi shear zone and the Ida Fault (Figure 1), may have been active at such early stage but overprinted by later movement. In contrast, the bulk

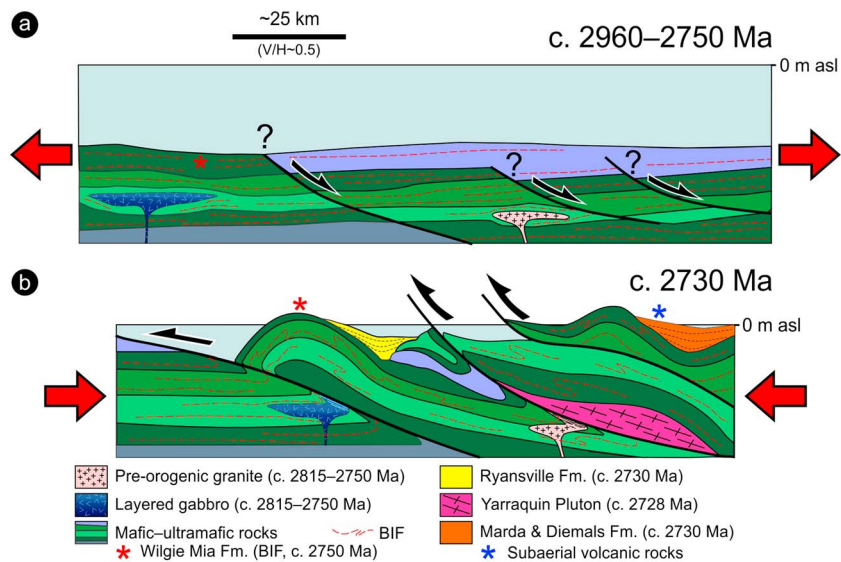


Figure 14. Cartoon outlining the pre- to early-orogenic evolution of the western part of the Yilgarn Orogen. (a) The 2960–2750 Ma period reflects the accumulation of a thick greenstone pile dominated by mafic-ultramafic volcanic rocks interlayered with BIFs, the latter devoid of any clastic input. It is likely that events of lithospheric extension during this period were accommodated by large-scale shear zones with normal kinematics. (b) At ~2730 Ma, the onset of the Neoarchean orogeny is marked by shearing along E dipping, large-scale contractional structures, exhumation of the 2960–2750 Ma succession to subaerial conditions, and proximal, high-energy sedimentary basins developed above a regional unconformity. At the same time, the Yarraquin pluton was emplaced along part of the wide network of contractional, E dipping shear zones.

of the post-2730 Ma regional deformation in the Murchison Domain was localized within two younger, large-scale syntectonic plutons (the Lakeside and Cundimurra plutons; Figure 4a [Zibra *et al.*, 2014a, 2014b]). This may account for the preservation of early-orogenic structures in the Yarraquin pluton.

Crustal thickening at the onset of the Yilgarn Orogeny is likely an expression of the progressive Neoarchean strengthening of the continental lithosphere, which produced a secular change in tectonic style and a transition from Archean-type to modern-type orogens [Rey and Coltice, 2008; Condie and O'Neill, 2010]. A genetic link between thrusting, large-scale rock uplift, and erosion has been recently documented for the mature tectonic stages of the Yilgarn Orogen [Zibra *et al.*, 2017] and applies to the tectonomagmatic and stratigraphic evolution described here.

In the Neoarchean Superior Province, lithosphere thickening during the 2750–2650 Ma orogeny that eventually led to continental collision [Percival *et al.*, 1994; Cruden *et al.*, 2006] was likely achieved through large-scale thrusting involving the upper mantle [Calvert and Ludden, 1999; Benn, 2006; van der Velden *et al.*, 2006]. Consistently, numerical modeling suggests that thrust stacking during the Late-Archean orogenic cycles might have been a viable way to generate the thick cratonic keel that assured long-term stability to Archean cratons [Cooper *et al.*, 2006]. When limiting the view to the crust, thermal modeling indicates that the cold and strong Yilgarn orogenic crust promptly recorded far-field stresses related to plate-scale tectonic interactions [Bodorkos and Sandiford, 2006]. The well-organized arrangement of dominantly E dipping tectonic slices that characterize the Yilgarn Craton (Figure 1c) is therefore an expression of the high integrated strength of the Neoarchean Yilgarn Orogen.

The bulk E-W horizontal shortening recorded during most of the tectonic evolution of the Yilgarn Orogen is commonly ascribed to a series of accretion episodes that led to amalgamation of the EGST, the Narryer and Southwest Terranes onto an older foreland represented by the Youanmi Terrane (Figures 1a–1c) [Myers, 1995; Wilde *et al.*, 1996; Barley *et al.*, 2008]. The Ida Fault is regarded as the suture between the EGST and the Youanmi Terrane [Myers, 1995], i.e., a scenario that is consistent with the existence of an ~2736–2724 Ma volcanic arc setting now preserved in the hangingwall of the Ida Fault (Figures 1b and 1c) [de Joux *et al.*, 2014], together with the occurrence of high-grade greenstones along this major structure (Figures 1b and 1c) [Zibra *et al.*, 2017]. Alternatively, the various terranes could have once been part of a Mesoarchean

“proto-Yilgarn” continent, subsequently rifted into a series of ribbon continents during possible extensional events within the ~2960–2750 Ma time slice, and in turn amalgamated again by inversion tectonics, during the Neoproterozoic Yilgarn Orogeny (autochthonous models [Czarnota *et al.*, 2010; Pawley *et al.*, 2012; Van Kranendonk *et al.*, 2013]). The latter model mainly hinges around the geochronological and isotopic evidence of broadly contemporaneous crust-forming events throughout the various terranes from at least ~3100 Ma [Wyche *et al.*, 2012; Mole *et al.*, 2014]. However, given that the Precambrian Earth recorded a series of global tectonomagmatic events [Barley *et al.*, 2005; O'Neill *et al.*, 2007], broadly contemporaneous crust-forming events could have been recorded even if the terranes now assembled into the Yilgarn Craton were not in physical contact.

In summary, available data sets allow for both end-member geodynamic models (accretion of an allochthonous EGST or inversion of an autochthonous ensialic rift) and both models may account for the tectonomagmatic and sedimentary evolution of the Yilgarn continent. Thus, many of the fundamental questions about Archean tectonics that have been raised since the 1970s [e.g., Kroner, 1977; Groves *et al.*, 1978; van Hunen *et al.*, 2008; Bédard *et al.*, 2013] still remain unanswered today.

Acknowledgments

We thank Olivier Vanderhaeghe, Steffen Büttner, and the Associate Editor Djordje Grujic for very constructive reviews that helped clarify the message and widen our views of orogenic processes. We also thank the Editor Nathan Niemi for prompt handling of the manuscript and for additional useful comments. R.H. Smithies helped with the compilation and interpretation of the geochemical data. P. Vota and T. Zama provided invaluable support during field work. M. Jones and M. Prause helped in preparing the figures. The staff of the GSWA laboratory prepared the samples for geochemistry analyses. S. Wyche provided useful comments on an earlier version of the manuscript. The paper is published with permission of the executive director of the Geological Survey of Western Australia. Additional data sets supporting our conclusions are included in the supporting information.

References

- Alexander, B. W., M. Bau, P. Andersson, and P. Dulski (2008), Continently-derived solutes in shallow Archean seawater: Rare Earth element and Nd isotope evidence in iron formation from the 2.9 Ga Pongola Supergroup, South Africa, *Geochim. Cosmochim. Acta*, 72(2), 378–394.
- Barley, M. E., B. N. Eisenlohr, D. I. Groves, C. S. Perring, and J. R. Vearncombe (1989), Late Archean convergent margin tectonics and gold mineralization: A new look at the Norseman-Wiluna Belt, Western Australia, *Geology*, 17(9), 826–829, doi:10.1130/0091-7613(1989)017<0826:LACMTA>2.3.CO;2.
- Barley, M., A. Bekker, and B. Krapež (2005), Late Archean to Early Paleoproterozoic global tectonics, environmental change and the rise of atmospheric oxygen, *Earth Planet. Sci. Lett.*, 238(1–2), 156–171, doi:10.1016/j.epsl.2005.06.062.
- Barley, M. E., S. J. A. Brown, B. Krapež, and N. Kositcin (2008), Physical volcanology and geochemistry of a Late Archaean volcanic arc: Kurnalpi and Gindalbie Terranes, Eastern Goldfields Superterrane, Western Australia, *Precambrian Res.*, 161(1), 53–76.
- Bédard, J., L. Harris, and P. Thurston (2013), The hunting of the snArc, *Precambrian Res.*, 229, 20–48.
- Benn, K. (2006), Tectonic delamination of the lower crust during Late Archean collision of the Abitibi—Opatita and Pontiac terranes, Superior Province, Canada, in *Archean Geodynamics and Environments*, pp. 267–282, AGU, Washington, D. C.
- Blumenfeld, P., D. Mainprice, and J. Bouchez (1986), C-slip in quartz from subsolidus deformed granite, *Tectonophysics*, 127, 97–155.
- Bodorkos, S., and M. Sandiford (2006), Thermal and mechanical controls on the evolution of Archean crustal deformation: Examples from Western Australia, in *Archean Geodynamics and Environments*, edited by K. Benn, J.-C. Mareschal, and K. C. Condie, pp. 131–147, AGU, Washington, D. C.
- Boger, S. D., and J. M. Miller (2004), Terminal suturing of Gondwana and the onset of the Ross–Delamerian Orogeny: The cause and effect of an Early Cambrian reconfiguration of plate motions, *Earth Planet. Sci. Lett.*, 219(1), 35–48.
- Calvert, A. J. A., and J. N. Ludden (1999), Archean continental assembly in the southeastern Superior Province of Canada, *Tectonics*, 18(3), 412–429, doi:10.1029/1999TC900006.
- Campbell, I. H., and R. I. Hill (1988), A two-stage model for the formation of the granite-greenstone terrains of the Kalgoorlie-Norseman area, Western Australia, *Earth Planet. Sci. Lett.*, 90(1), 11–25, doi:10.1016/0012-821X(88)90107-0.
- Cesare, B., C. Marchesi, and J. A. D. Connolly (2002), Growth of myrmekite coronas by contact metamorphism of granitic mylonites in the aureole of Cima di Vila, Eastern Alps, Italy, *J. Metamorph. Geol.*, 20(1), 203–213.
- Champion, D. C., and R. H. Smithies (2007), Geochemistry of Paleoproterozoic granites of the East Pilbara Terrane, Pilbara Craton, Western Australia: Implications for early Archean crustal growth, *Dev. Precambrian Geol.*, 15, 369–409, doi:10.1016/S0166-2635(07)15043-X.
- Champion, D. C. D., and J. J. W. Sheraton (1997), Geochemistry and Nd isotope systematics of Archaean granites of the Eastern Goldfields, Yilgarn Craton, Australia: Implications for crustal growth processes, *Precambrian Res.*, 83(1–3), 109–132, doi:10.1016/S0301-9268(97)00007-7.
- Chen, S., J. Libby, J. Greenfield, S. Wyche, and A. Riganti (2001), Geometry and kinematics of large arcuate structures formed by impingement of rigid granitoids into greenstone belts during progressive shortening, *Geology*, 29(3), 283–286.
- Chen, S., A. Riganti, S. Wyche, and J. Greenfield (2003), Lithostratigraphy and tectonic evolution of contrasting greenstone successions in the central Yilgarn Craton, Western Australia, *Precambrian Res.*, 127, 249–266.
- Chew, D. M., J. R. Graham, and M. J. Whitehouse (2007), U–Pb zircon geochronology of plagiogranites from the Lough Nafooy (=Midland Valley) arc in western Ireland: Constraints on the onset of the Grampian orogeny, *J. Geol. Soc. Lond.*, 164(4), 747–750.
- Cohalan, L., R. F. Weinberg, R. J. Squire, and C. M. Allen (2015), Early deformation in the Eastern Goldfields, Yilgarn Craton, Western Australia: A record of early thrusting?, *Precambrian Res.*, 266(266), 212–226, doi:10.1016/j.precamres.2015.05.013.
- Collins, W. (1989), Polydiapirism of the Archean Mount Edgar Batholith, Pilbara Block, Western Australia, *Precambrian Res.*, 43(1–2), 41–62.
- Condie, K. (1990), Geochemical characteristics of Precambrian basaltic greenstones, in *Early Precambrian Basic Magmatism*, edited by R. P. Hall and D. J. Hughes, pp. 40–55, Blackie, Glasgow.
- Condie, K. C., and K. Benn (2006), Archean geodynamics: Similar to or different from modern geodynamics?, *Archean Geodyn. Environ.*, 47–59.
- Condie, K. C., and C. O'Neill (2010), The Archean-Proterozoic boundary: 500 My of tectonic transition in Earth history, *Am. J. Sci.*, 310(9), 775–790, doi:10.2475/09.2010.01.
- Cooper, C. M., A. Lenardic, A. Levander, and L. Moresi (2006), Creation and preservation of cratonic lithosphere: Seismic constraints and geodynamic models, in *Archean Geodynamics and Environments*, edited by K. Benn, J.-C. Mareschal, and K. C. Condie, pp. 75–88, AGU, Washington, D. C.
- Corcoran, P., and W. Mueller (2007), Time-transgressive Archean unconformities underlying molasse basin-fill successions of dissected oceanic arcs, Superior Province, Canada, *J. Geol.*, 120(1), 177–203.

- Cruden, A., M. Nasser, and R. Pysklywec (2006), Surface topography and internal strain variation in wide hot orogens from three-dimensional analogue and two-dimensional numerical vice models, *Geol. Soc. London, Spec.*, 253(1), 79–104.
- Czarnota, K., D. D. C. Champion, B. Goscombe, R. S. Blewett, K. F. Cassidy, P. A. Henson, and P. B. Groenewald (2010), Geodynamics of the eastern Yilgarn Craton, *Precambrian Res.*, 183(2), 175–202, doi:10.1016/j.precamres.2010.08.004.
- Dalstra, H. J., J. R. Ridley, E. J. M. Bloem, and D. I. Groves (1999), Metamorphic evolution of the central Southern Cross Province, Yilgarn Craton, Western Australia, *Aust. J. Earth Sci.*, 46(5), 765–784.
- DeCelles, P., G. Gehrels, Y. Najman, and A. Martin (2004), Detrital geochronology and geochemistry of Cretaceous–Early Miocene strata of Nepal: Implications for timing and diachroneity of initial Himalayan orogenesis, *Earth Planet. Sci. Lett.*, 227, 313–330.
- de Joux, A., T. Thordarson, J. G. Fitton, and A. R. Hastie (2014), The Cosmos greenstone succession, Agnew–Wiluna greenstone belt, Yilgarn Craton, Western Australia: Geochemistry of an enriched Neoproterozoic volcanic arc succession, *Lithos*, 205, 148–167, doi:10.1016/j.lithos.2014.06.013.
- Dieni, I., and F. Massari (1982), Présence de glaucophane détritique dans le Maastrichtien inférieur de Sardaigne orientale. Implications géodynamiques, *CR Acad. Sc. Paris*, 295, 679–682.
- Drummond, B. J., B. R. Goleby, and C. P. Swager (2000), Crustal signature of Late Archaean tectonic episodes in the Yilgarn craton, Western Australia: Evidence from deep seismic sounding, *Tectonophysics*, 329(1–4), 193–221, doi:10.1016/S0040-1951(00)00196-7.
- Flament, N., P. Rey, N. Coltice, G. Dromart, and N. Olivier (2011), Lower crustal flow kept Archean continental flood basalts at sea level, *Geology*, 39(12), 1159–1162.
- Gapais, D., and B. Barbarin (1986), Quartz fabric transition in a cooling syntectonic granite (Hermitage Massif, France), *Tectonophysics*, 125, 357–370.
- Garzanti, E., A. Baud, and G. Mascle (1987), Sedimentary record of the northward flight of India and its collision with Eurasia (Ladakh Himalaya, India), *Geodin. Acta*, 1, 297–312.
- Gee, R. D., J. L. Baxter, S. A. Wilde, and I. R. Williams (1981), Crustal development in the Archaean Yilgarn Block, Western Australia, *Spec. Publ. Geol. Soc. Aust.*, 7, 43–56.
- Gerya, T. (2014), Precambrian geodynamics: Concepts and models, *Gondwana Res.*, 25(2), 442–463.
- Gilbert, G. K. (1890), *Lake Bonneville, US Geol. Surv. Monogr.*, 438 pp., US Gov. Print. Off., Washington, D. C.
- Goleby, B. R., R. S. Blewett, R. J. Korsch, D. C. Champion, K. F. Cassidy, L. E. A. Jones, P. B. Groenewald, and P. Henson (2004), Deep seismic reflection profiling in the Archaean northeastern Yilgarn Craton, Western Australia: Implications for crustal architecture and mineral potential, *Tectonophysics*, 388(1–4), 119–133, doi:10.1016/j.tecto.2004.04.032.
- Goodwin, L., and B. Tikoff (2002), Competency contrast, kinematics, and the development of foliations and lineations in the crust, *J. Struct. Geol.*, 24, 1065–1085.
- Gower, R. J. W., and C. Simpson (1992), Phase boundary mobility in naturally deformed, high-grade quartzofeldspathic rocks: Evidence for diffusional creep, *J. Struct. Geol.*, 14(3), 301–313.
- Groves, D. I., N. J. Archibald, L. F. Bettenay, and R. A. Binns (1978), Greenstone belts as ancient marginal basins or ensialic rift zones, *Nature*, 273(5662), 460–461, doi:10.1038/273460a0.
- Hamilton, W. (1998), Archean magmatism and deformation were not products of plate tectonics, *Precambrian Res.*, 91(1–2), 143–179.
- Hammes, D. M., and M. Petermann (2016), FAME: Software for analysing rock microstructures, *Comput. Geosci.*, 90, 24–33.
- Handy, M., S. Schmid, R. Bousquet, and E. Kissling (2010), Reconciling plate-tectonic reconstructions of Alpine Tethys with the geological–geophysical record of spreading and subduction in the Alps, *Earth Sci. Rev.*, 102(3), 121–158.
- Haugaard, R., L. Ootes, and K. Konhauser (2017), Neoproterozoic banded iron formation within a ~2620 Ma turbidite-dominated deep-water basin, Slave craton, NW Canada, *Precambrian Res.*, 292, 130–151.
- Hayman, P., N. Thébaud, M. Pawley, and S. Barnes (2015), Evolution of a ~2.7 Ga large igneous province: A volcanological, geochemical and geochronological study of the Agnew Greenstone Belt, and new regional, *Precambrian Res.*, 270, 334–368.
- Hibbard, M. J. (1987), Deformation of incompletely crystallized magma systems: Granitic gneisses and their tectonic implications, *J. Geol.*, 95(4), 543–561.
- Hippert, J., A. Rocha, C. Lana, M. Egydio-Silva, and T. Takeshita (2001), Quartz plastic segregation and ribbon development in high-grade striped gneisses, *J. Struct. Geol.*, 23(1), 67–80.
- Hopson, R. F., and K. Rarnseyer (1990), Cathodoluminescence microscopy of myrmekite, *Geology*, 18(4), 336–339.
- Hu, X., E. Garzanti, T. Moore, and I. Raffi (2015), Direct stratigraphic dating of India–Asia collision onset at the Selandian (middle Paleocene, 59 ± 1 Ma), *Geology*, 43(10), 859–862.
- Ivanic, T. J., M. J. Van Kranendonk, C. L. Kirkland, S. Wyche, M. T. D. Wingate, and E. A. Belousova (2012), Zircon Lu–Hf isotopes and granite geochemistry of the Murchison Domain of the Yilgarn Craton: Evidence for reworking of Eoarchean crust during Meso–Neoproterozoic plume-driven magmatism, *Lithos*, 148, 112–127, doi:10.1016/j.lithos.2012.06.006.
- Johnson, T. E., M. Brown, N. J. Gardiner, C. L. Kirkland, and R. H. Smithies (2017), Earth’s first stable continents did not form by subduction, *Nature*, 543(7644), 239–242, doi:10.1038/nature21383.
- Jones, R., R. Holdsworth, P. Clegg, and K. McCaffrey (2004), Inclined transpression, *J. Struct. Geol.*, 26, 1531–1548.
- Kamber, B. S., A. Greig, and K. D. Collerson (2005), A new estimate for the composition of weathered young upper continental crust from alluvial sediments, Queensland, Australia, *Geochim. Cosmochim. Acta*, 69(4), 1041–1058.
- Klein, C. (2005), Some Precambrian banded iron-formations (BIFs) from around the world: Their age, geologic setting, mineralogy, metamorphism, geochemistry, and origin, *Am. Mineral.*, 90(10), 1473–1499.
- Krapež, B., and M. Barley (2008), Late Archaean synorogenic basins of the Eastern Goldfields Superterrane, Yilgarn Craton, Western Australia: Part III. Signatures of tectonic escape in an arc-continent, *Precambrian Res.*, 161(1), 183–199.
- Kroner, A. (1977), Precambrian mobile belts of southern and eastern Africa—Ancient sutures or sites of ensialic mobility? a case for crustal evolution toward plate tectonics, *Tectonophysics*, 40(1–2), 101–135, doi:10.1016/0040-1951(77)90031-2.
- Kruhl, J. H. (1996), Prism- and basal-plane parallel subgrain boundaries in quartz: A microstructural geothermobarometer, *J. Metamorph. Geol.*, 14(5), 581–589.
- Lamb, S. (1987), Archean synsedimentary tectonic deformation—A comparison with the Quaternary, *Geology*, 15(6), 565, doi:10.1130/0091-7613(1987)15<565:ASTDCW>2.0.CO;2.
- Lu, Y., M. T. D. Wingate, and I. Zibra (2016), 155510. Granodiorite dyke, Fred Bore. Geochronology Record 1347: Geological Survey of Western Australia. [Available at: <http://geodocs.dmp.wa.gov.au/search.jsp?documentId=631171>.]
- Mainprice, D., J. Bouchez, P. Blumenfeld, and J. Tubià (1986), Dominant c slip in naturally deformed quartz: Implications for dramatic plastic softening at high temperature, *Geology*, 14, 819–822.

- Martin, H., R. H. H. Smithies, R. Rapp, J.-F. J.-F. Moyon, and D. Champion (2005), An overview of adakite, tonalite–trondhjemite–granodiorite (TTG), and sanukitoid: Relationships and some implications for crustal evolution, *Lithos*, 79(1), 1–24, doi:10.1016/j.lithos.2004.04.048.
- Menegon, L., G. Pennacchioni, and H. Stünitz (2006), Nucleation and growth of myrmekite during ductile shear deformation in metagranites, *J. Metamorph. Geol.*, 24(7), 553–568.
- Menegon, L., G. Pennacchioni, and R. Spiess (2008), Dissolution-precipitation creep of K-feldspar in mid-crustal granite mylonites, *J. Struct. Geol.*, 30(5), 565–579.
- Mole, D. R., et al. (2014), Crustal evolution, intra-cratonic architecture and the metallogeny of an Archaean craton, *Geol. Soc. Spec. Publ.*, 393(1), 23–80, doi:10.1144/SP393.8.
- Morris, P., and C. Kirkland (2014), Melting of a subduction-modified mantle source: A case study from the Archean Marda Volcanic Complex, central Yilgarn Craton, Western Australia, *Lithos*, 190, 403–419.
- Morris, P. A., A. Riganti, and S. F. Chen (2007), Evaluating the provenance of Archean sedimentary rocks of the Diemals Formation (central Yilgarn Craton) using whole-rock chemistry and precise U–Pb zircon chronology, *Aust. J. Earth Sci.*, 54(8), 1123–1136.
- Moyon, J.-F. (2011), The composite Archean grey gneisses: Petrological significance, and evidence for a non-unique tectonic setting for Archean crustal growth, *Lithos*, 123(1–4), 21–36, doi:10.1016/j.lithos.2010.09.015.
- Moyon, J.-F., and H. Martin (2012), Forty years of TTG research, *Lithos*, 148, 312–336, doi:10.1016/j.lithos.2012.06.010.
- Mueller, W., and P. Corcoran (1998), Late-orogenic basins in the Archean Superior Province, Canada: Characteristics and inferences, *Sediment. Geol.*, 120(1), 177–203.
- Myers, J. S. (1995), The generation and assembly of an Archean supercontinent: Evidence from the Yilgarn craton, Western Australia, *Geol. Soc. London, Spec. Publ.*, 95(1), 143–154, doi:10.1144/GSL.SP.1995.095.01.09.
- Najman, Y., et al. (2010), Timing of India-Asia collision: Geological, biostratigraphic, and palaeomagnetic constraints, *J. Geophys. Res.*, 115, B12416, doi:10.1029/2010JB007673.
- O'Neill, C., A. Lenardic, L. Moresi, T. H. Torsvik, and C.-T. A. Lee (2007), Episodic Precambrian subduction, *Earth Planet. Sci. Lett.*, 262(3–4), 552–562, doi:10.1016/j.epsl.2007.04.056.
- Passchier, C., and S. Coelho (2006), An outline of shear-sense analysis in high-grade rocks, *Gondwana Res.*, 10(1–2), 66–76, doi:10.1016/j.gr.2005.11.016.
- Passchier, C. W., and R. A. J. Trouw (2005) *Microtectonics*, 2nd ed., Springer, Berlin.
- Paterson, S. R., R. H. Vernon, and O. T. Tobisch (1989), A review of criteria for the identification of magmatic and tectonic foliations in granitoids, *J. Struct. Geol.*, 11(3), 349–363.
- Pawley, M. J., M. T. D. Wingate, C. L. Kirkland, S. Wyche, C. E. Hall, S. S. Romano, and M. P. Doublier (2012), Adding pieces to the puzzle: Episodic crustal growth and a new terrane in the northeast Yilgarn Craton, Western Australia, *Aust. J. Earth Sci.*, 59(5), 603–623, doi:10.1080/08120099.2012.696555.
- Percival, J. A., R. A. Stern, T. Skulski, K. D. Card, J. K. Mortensen, and N. J. Bégin (1994), Minto block, Superior province: Missing link in deciphering assembly of the craton at 2.7 Ga, *Geology*, 22(9), 839, doi:10.1130/0091-7613(1994)022<0839:MBSPML>2.3.CO;2.
- Peternell, M., P. Hasalová, C. J. L. Wilson, S. Piazzolo, and K. Schulmann (2010), Evaluating quartz crystallographic preferred orientations and the role of deformation partitioning using EBSD and fabric analyser techniques, *J. Struct. Geol.*, 32(6), 803–817.
- Peternell, M., M. Dierckx, C. J. L. Wilson, and S. Piazzolo (2014), Quantification of the microstructural evolution of polycrystalline fabrics using FAME: Application to in situ deformation of ice, *J. Struct. Geol.*, 61, 109–122.
- Phillips, E. (1974), Myrmekite—one hundred years later, *Lithos*, 7, 181–194.
- Qiu, Y., and D. I. Groves (1999), Late Archean collision and delamination in the Southwest Yilgarn Craton; the driving force for Archean orogenic lode gold mineralization?, *Econ. Geol.*, 94(1), 115–122, doi:10.2113/gsecongeo.94.1.115.
- Qiu, Y. M., N. J. McNaughton, D. I. Groves, and H. J. Dalstra (1999), Ages of internal granitoids in the Southern Cross region, Yilgarn Craton, Western Australia, and their crustal evolution and tectonic implications, *Aust. J. Earth Sci.*, 46(6), 971–981, doi:10.1046/j.1440-0952.1999.00758.x.
- Rey, P. F., and N. Coltice (2008), Neoproterozoic lithospheric strengthening and the coupling of Earth's geochemical reservoirs, *Geology*, 36(8), 635, doi:10.1130/G25031A.1.
- Riganti, A., and S. Chen (2000), Geology of the Jackston 1:100 000 sheet: Western Australia Geological Survey, 1:100 000 Geological Series Explanatory Notes, 51 p. [Available at <http://dmpbookshop.eruditetechnologies.com.au/product/geology-of-the-jackson-1100-000-sheet.do>.]
- Rosenberg, C., and M. Handy (2005), Experimental deformation of partially melted granite revisited: Implications for the continental crust, *J. Metamorph. Geol.*, 23, 19–28.
- Rosenberg, C., and U. Riller (2000), Partial-melt topology in statically and dynamically recrystallized granite, *Geology*, 28, 7–10.
- Rudnick, R. L., and S. Gao (2003), Composition of the continental crust, *Treat. Geochem.*, 3, 659.
- Sawyer, E. (2000), Grain-scale and outcrop-scale distribution and movement of melt in a crystallising granite, *Geol. Soc. Am. Spec. Pap.*, 350, 73–85.
- Schellart, W. P., and N. Rawlinson (2010), Convergent plate margin dynamics: New perspectives from structural geology, geophysics and geodynamic modelling, *Tectonophysics*, 483(1–2), 4–19, doi:10.1016/j.tecto.2009.08.030.
- Schiette, L., and I. H. Campbell (1996), Chronology of the Mount Magnet granite-greenstone terrain, Yilgarn Craton, Western Australia: Implications for field based predictions of the relative timing of granitoid emplacement, *Precambrian Res.*, 78(4), 237–260, doi:10.1016/0301-9268(95)00064-X.
- Schmid, S., and M. Casey (1986), Complete fabric analysis of some commonly observed quartz c-axis patterns, *Miner. Rock Deform. Lab. Stud.*, 36, 263–286.
- Simpson, C., and R. P. Wirth (1989), Evidence for deformation-induced K-feldspar replacement by myrmekite, *J. Metamorph. Geol.*, 7(2), 261–275.
- Squire, R., C. Allen, R. Cas, and I. Campbell (2010), Two cycles of voluminous pyroclastic volcanism and sedimentation related to episodic granite emplacement during the late Archean: Eastern Yilgarn Craton, Western Australia, *Precambrian Res.*, 183, 251–274.
- Stampfli, G., G. Borel, R. Marchant, and J. Mosar (2002), Western Alps geological constraints on western Tethyan reconstructions, *J. Virtual Explor.*, 8, 77.
- Stipp, M., H. Stünitz, R. Heilbronner, and S. M. Schmid (2002), The eastern Tonale fault zone: A “natural laboratory” for crystal plastic deformation of quartz over a temperature range from 250 to 700 °C, *J. Struct. Geol.*, 24(12), 1861–1884.
- Swager, C., and D. Nelson (1997), Extensional emplacement of a high-grade granite gneiss complex into low-grade greenstones, Eastern Goldfields, Yilgarn Craton, Western Australia, *Precambrian Res.*, 83, 203–219.

- Thompson, M., R. Watchorn, C. Bonwick, and M. Frewin (1990), Gold deposits of Hill 50 Gold Mine NL at Mount Magnet, in *Geology of the Mineral Deposits of Australia and Papua New Guinea*, edited by F. E. Hughes, pp. 221–241, The Australasian Institute of Mining and Metallurgy, Melbourne.
- Thurston, P., B. Kamber, and M. Whitehouse (2012), Archean cherts in banded iron formation: Insight into Neoproterozoic ocean chemistry and depositional processes, *Precambrian Res.*, *214*, 227–257.
- Thurston, P. C., and K. M. Chivers (1990), Secular variation in greenstone sequence development emphasizing Superior Province, Canada, *Precambrian Res.*, *46*(1–2), 21–58.
- Tikoff, B., and D. Greene (1997), Stretching lineations in transpressional shear zones: An example from the Sierra Nevada Batholith, California, *J. Struct. Geol.*, *19*(1), 29–39, doi:10.1016/S0191-8141(96)00056-9.
- Vanderhaeghe, O. (2012), The thermal–mechanical evolution of crustal orogenic belts at convergent plate boundaries: A reappraisal of the orogenic cycle, *J. Geodyn.*, *56*–57, 124–145, doi:10.1016/j.jog.2011.10.004.
- Vearncombe, J. (1998), Shear zones, fault networks, and Archean gold, *Geology*, *26*(9), 855–858.
- van der Velden, A. J., F. A. Cook, B. J. Drummond, and B. R. Goleby (2006), Reflections of the Neoproterozoic: A global perspective, in *Archean Geodynamics and Environments*, edited by K. Benn, J.-C. Mareschal, and K. C. Condie, pp. 255–265, AGU, Washington, D. C.
- van Hunen, J., P. E. van Keken, A. Hynes, and G. F. Davies (2008), Tectonics of early Earth: Some geodynamic considerations, *Geol. Soc. Am. Spec. Pap.*, *440*, 157–171, doi:10.1130/2008.2440(08).
- Van Kranendonk, M. J., T. J. Ivanic, M. T. D. Wingate, C. L. Kirkland, and S. Wyche (2013), Long-lived, autochthonous development of the Archean Murchison Domain, and implications for Yilgarn Craton tectonics, *Precambrian Res.*, *229*, 49–92.
- Vernon, R. H. (2000), Review of microstructural evidence of magmatic and solid-state flow, *Vis. Geosci.*, *5*(2), 1–23.
- Vigneresse, J. L., and B. Tikoff (1999), Strain partitioning during partial melting and crystallizing felsic magmas, *Tectonophysics*, *312*(2), 117–132.
- Wang, Q., L. S. Tte, and I. Campbell (1998), Geochronology of supracrustal rocks from the Golden Grove area, Murchison Province, Yilgarn Craton, Western Australia, *Aust. J. Earth Sci.*, *45*, 571–577.
- Weinberg, R. F., L. Moresi, and P. van der Borgh (2003), Timing of deformation in the Norseman-Wiluna belt, Yilgarn craton, Western Australia, *Precambrian Res.*, *120*(3), 219–239.
- Wilde, S. A., M. F. Middleton, and B. J. Evans (1996), Terrane accretion in the southwestern Yilgarn Craton: Evidence from a deep seismic crustal profile, *Precambrian Res.*, *78*(1–3), 179–196.
- Wilson, C. J. L., D. S. Russell-Head, K. Kunze, and G. Viola (2007), The analysis of quartz c-axis fabrics using a modified optical microscope, *J. Microsc.*, *227*(1), 30–41, doi:10.1111/j.1365-2818.2007.01784.x.
- Wingate, M. T. D., C. L. Kirkland, and I. Zibra (2014), 155511: granodiorite gneiss, Top Camp Well. Geochronology Record 1169: Geological Survey of Western Australia. [Available at <http://geodocs.dmp.wa.gov.au/search.jsp?documentId=465759>, Perth].
- Wyche, S. (2007), Evidence of Pre-3100 Ma Crust in the Youanmi and South West Terranes, and Eastern Goldfields Superterrane, of the Yilgarn Craton, *Dev. Precambrian Geol.*, *15*, 113–123.
- Wyche, S., S. F. Chen, J. E. Greenfield, and A. Riganti (2001), Geology of the Johnston Range 1:100 000 sheet: Western Australia Geological Survey, 1:100 000 Geological Series Explanatory Notes, 31p. [Available at <http://dmpbookshop.eruditetechnologies.com.au/product/geology-of-the-johnston-range-1100-000-sheet.do>, Perth].
- Wyche, S., C. L. Kirkland, A. Riganti, M. J. Pawley, E. Belousova, and M. T. D. Wingate (2012), Isotopic constraints on stratigraphy in the central and eastern Yilgarn Craton, Western Australia, *Aust. J. Earth*, *59*(5), 657–670, doi:10.1080/08120099.2012.697677.
- Wyche, S., T. Ivanic, and I. Zibra (2013), Youanmi and Southern Carnarvon seismic and magnetotelluric (MT) workshop 2013. Geological Survey of Western Australia, Record 6, 180 p. [Available at <http://dmpbookshop.eruditetechnologies.com.au/product/youanmi-and-southern-carnarvon-seismic-and-magnetotelluric>].
- Zibra, I. (2015), Mount Magnet, WA Sheet 2241: Geological Survey of Western Australia, 1:100 000 Geological Series. [Available at <http://dmpbookshop.eruditetechnologies.com.au/product/mount-magnet-wa-sheet-2241.do>, Perth].
- Zibra, I., J. Kruhl, and R. Braga (2010), Late Palaeozoic deformation of post-Variscan lower crust: Shear zone widening due to strain localization during retrograde shearing, *Int. J. Earth Sci.*, *99*, 973–991.
- Zibra, I., J. Kruhl, A. Montanini, and R. Tribuzio (2012), Shearing of magma along a high-grade shear zone: Evolution of microstructures during the transition from magmatic to solid-state flow, *J. Struct. Geol.*, *37*, 150–160.
- Zibra, I., T. J. Ivanic, and S. F. Chen (2013), Wynyangoo, WA Sheet 2542: Geological Survey of Western Australia, 1:100 000 Geological Series. [Available at <http://dmpbookshop.eruditetechnologies.com.au/product/wynyangoo-wa-sheet-2542.do>, Perth].
- Zibra, I., R. H. Smithies, M. T. D. Wingate, and C. L. Kirkland (2014a), Incremental pluton emplacement during inclined transpression, *Tectonophysics*, *623*, 100–122.
- Zibra, I., K. Gessner, H. R. Smithies, and M. Peternell (2014b), On shearing, magmatism and regional deformation in Neoproterozoic granite-greenstone systems: Insights from the Yilgarn Craton, *J. Struct. Geol.*, *67*, 253–267, doi:10.1016/j.jsg.2013.11.010.
- Zibra, I., T. Ivanic, S. Chen, and F. Clos (2016), Badja, WA Sheet 2240: Geological Survey of Western Australia, 1:100 000 Geological Series. [Available at <http://dmpbookshop.eruditetechnologies.com.au/product/badja-wa-sheet-2240.do>, Perth].
- Zibra, I., F. J. Korhonen, M. Peternell, R. Weinberg, S. S. Romano, R. Braga, M. De Paoli, and M. Roberts (2017), On thrusting, regional unconformities and exhumation of high-grade greenstones in Neoproterozoic orogens. The case of the Waroonga Shear Zone, Yilgarn Craton, *Tectonophysics*, doi:10.1016/j.tecto.2017.05.017.